SYNTHESIS OF RARE EARTH COMPOUNDS AND STUDY OF THEIR MAGNETIC OPTICAL AND SEMICONDUCTING PROPERTIES

IBM Corporation
Thomas J. Watson Research Center
Yorktown Heights, New York 10598

FINAL TECHNICAL REPORT

June 1971

Contract No. DAAH01-70-C-1309
Program Code No. 0D10

sponsored by

Advanced Research Project Agency
ARPA Order No. 1588

ARPA Support Office - Army Missile Command
Directorate for Research, Development,
Engineering and Missile Systems Laboratory
U.S. Army Missile Command
Redstone Arsenal, Alabama

81

DOCUMENT CONTROL DATA - R & D

(Security classification of title, body of abstract and indexing annotation must be entered when the overall report is classified)

1. ORIGINATING ACTIVITY *(Corporate author)*
International Business Machines Corporation
Thomas J. Watson Research Center, P. O. Box 218
Yorktown Heights, New York 10598

2a. REPORT SECURITY CLASSIFICATION
Unclassified

2b. GROUP

3. REPORT TITLE

RESEARCH IN THE SYNTHESIS OF RARE EARTH COMPOUNDS AND A STUDY OF THEIR MAGNETIC OPTICAL AND SEMICONDUCTING PROPERTIES

4. DESCRIPTIVE NOTES *(Type of report and inclusive dates)*
Final Technical Report (30 June 1970 to 30 June 1971)

5. AUTHOR(S) *(First name, middle initial, last name)*

F. Holtzberg, T. R. McGuire, T. Penney, M. W. Shafer and S. von Molnar

6. REPORT DATE June 71	7a. TOTAL NO. OF PAGES 80	7b. NO. OF REFS 57

8a. CONTRACT OR GRANT NO.
DAAH01-70-C-1309
b. PROJECT NO.

c. Program Code No. OD10

d.

9a. ORIGINATOR'S REPORT NUMBER(S)
IBM Project # 2533

9b. OTHER REPORT NO(S) *(Any other numbers that may be assigned this report)*

10. DISTRIBUTION STATEMENT

Distribution of this document is unlimited

11. SUPPLEMENTARY NOTES

12. SPONSORING MILITARY ACTIVITY
Advanced Research Project Agency
Arlington, Virginia 22209
ARPA Order No. 1588

13. ABSTRACT

Considerable information has been obtained on the nature of vapor-solid equilibria in EuO, EuS and EuSe. Crystal growth experiments and Knudsen effusion with mass spectrometric analyses show that EuS and EuSe vaporize to yield essentially equal pressures of Eu and chalcogen in the vapor phase. In contrast EuO has been shown to be in equilibrium with only Eu vapor. With this information it has been possible to significantly improve the growth conditions and the purity and perfection of single crystals. One important consequence has been a meaningful correlation of sample preparation with physical properties.

A study of the reaction between H_2S and Eu_2O_3 was carried out to determine the amount of residual oxygen in EuS as a function of reaction temperature. Samples produced at 1250-1300°C in flowing H_2S were found to contain less than 75 ppm oxygen. The use of this material resulted in the growth of more perfect EuS single crystals with a significantly lower oxygen content.

Magnetic measurements for the system $Eu_{1-x}Gd_xS$ show ferromagnetic properties with temperatures up to three times that of insulating EuS. Surprisingly, however, the low temperature saturation moment decreases with Gd concentration. This decrease in moment is believed to reflect the development of a canted magnetic structure.

We have shown that the glass forming region in divalent europium chalcogenides can be extended beyond 50 mole % EuO and that it is possible to introduce trivalent rare earth metals as potential dopants into these systems.

It has been demonstrated that the insulator-metal transition found in EuO is caused by an exponentially changing carrier concentration with an activation energy which decreases linearly with increasing magnetization.

14. KEY WORDS	LINK A		LINK B		LINK C	
	ROLE	WT	ROLE	WT	ROLE	WT
Semiconducting ferromagnets						
Europium chalcogenides						
Synthesis						
Nonstoichiometry						
Photoconductivity						
Crystal growth						
Rare earths						
Insulator-metal transition						

NOTICE

"This research was sponsored by the Advanced Research Projects Agency of the Department of Defense under ARPA Order No. 1588 and was monitored by the U. S. Army Missile Command under Contract No. DAAH01-70-C-1309. Views and conclusions expressed herein are the primary responsibility of the author or the contractor and should not be interpreted as representing the official opion or policy of USAMICOM. ARPA, DOD or any other agency of the Government."

BLANK PAGE

SYNTHESIS OF RARE EARTH COMPOUNDS AND STUDY OF THEIR MAGNETIC OPTICAL AND SEMICONDUCTING PROPERTIES

IBM Corporation
Thomas J. Watson Research Center
Yorktown Heights, New York 10598

FINAL TECHNICAL REPORT

June 1971

Contract No. DAAH01-70-C-1309
Program Code No. 0D10

sponsored by

Advanced Research Project Agency
ARPA Order No. 1588

ARPA Support Office - Army Missile Command
Directorate for Research, Development,
Engineering and Missile Systems Laboratory
U.S. Army Missile Command
Redstone Arsenal, Alabama

FOREWORD

This report describes work performed under contract DAAH01-70-C-1309 for the ARPA Support Office, Research, Development, Engineering and Missiles Laboratory, U. S. Army Missile Command, Redstone Arsenal, Alabama during the period 30 June 1970 through 30 June 1971. The monitors for this project were R. Norman and S. L. Johnston. The principal investigator was F. Holtzberg and the report was written by F. Holtzberg, T. R. McGuire, T. Penney, M. W. Shafer and S. von Molnar. The work was performed at the IBM Thomas J. Watson Research Center. The authors gratefully acknowledge the technical assistance of E. D. Battista, R. A. Figat, H. R. Lilienthal, P. G. Lockwood and J. M. Rigotty.

SUMMARY

We have emphasized the development of an understanding of the chemical equilibria involved in the synthesis and crystal growth of pure and doped europium chalcogenides. We have also further explored the relationship of defect structures and dopant concentration to the magnetic, optical and transport properties of these materials.

Since nonstoichiometry is a significant factor determining the physical properties of the chalcogenides, vapor-solid equilibria in EuO, EuSe and EuS were investigated. Knudsen effusion and mass spectrometric analyses show that EuSe and EuS dissociate to yield essentially equal pressures of Eu and chalcogen in the vapor phase. In contrast EuO has been shown to be in equilibrium with only Eu vapor. This information made possible the establishment of the conditions for single crystal growth. One important consequence of this has been a meaningful correlation of sample preparation with physical properties.

A study of the reaction between H_2S and Eu_2O_3 was carried out to determine the amount of residual oxygen in EuS as a function of reaction temperature. Samples produced at 1250-1300°C in flowing H_2S were found to contain less than 75 ppm oxygen. The use of this material resulted in the growth of more perfect EuS single crystals with a significantly lower oxygen content.

Magnetic measurements for the system $Eu_{1-x}Gd_xS$ show ferromagnetic properties with Curie temperatures up to three times that of insulating EuS. Surprisingly, however, the low temperature saturation moment decreases with Gd concentration. This decrease in moment is believed to reflect the development of a canted magnetic structure.

Transport properties in both metallic and semiconducting europium chalcogenides have been investigated. In the former the effort was directed toward understanding the exchange interactions between conduction electrons and the localized spin of the rare earths. In the latter, the purpose was to understand the conduction process and its dependence on magnetization and impurity concentration. One technique which has been particularly successful is photoconductivity. The results of static and transient photoconductivity measurements in EuSe show that just as in lightly doped EuSe:Gd there is thermally activated conduction in the paramagnetic region which increases with increasing magnetic field. The thermally activated conduction may be due to either hopping or thermal excitation to the conduction band. The activation energy is magnetic in origin.

We have also shown that the insulator-metal transition in EuO:Eu may be understood in terms of thermally activated carriers and an activation energy linearly dependent on magnetization both with and without an external magnetic field. The data are not consistent with an interpretation based on short range order.

TABLE OF CONTENTS

Page

LIST OF FIGURES

LIST OF TABLES

1.0 INTRODUCTION

The magnetic, optical, and electrical properties of the semiconducting ferromagnetic europium monochalcogenides have been shown to be critically dependent on electron concentration. The stoichiometric compounds are insulators with resistivities of the order of 10^8 to 10^{10} Ω-cm. The electron concentration can be varied by doping with trivalent rare earths, halide ions, or by developing vacancies on the anion or cation sites. At concentrations of about 1%, or 10^{19} carriers per cc, the chalcogenides are essentially metallic if compensation does not occur. Since single crystals of the monochalcogenide compounds are grown at very high temperatures (2000-2500°C) in sealed tungsten crucibles, the stoichiometry of the compound will be strongly dependent on the partial pressures and the composition of the vapor species, on the thermal history of the crystal as the temperature is reduced to ambient, and on the inclusion of impurities not segregated during the crystallization process. The concentration of impurities and dopants can be chemically measured to a level of several atomic parts per million using electron probe and mass spectrometric techniques. What cannot be measured readily from a chemical viewpoint is the degree of compensation or the vacancy concentration on either lattice site. Investigation of these materials therefore depends critically on correlation of the conditions used for the growth of single crystals with physical measurements, in order to develop insight into the nature of the defect structures.

With this in mind we established the following objectives:

1. To determine the nature of solid-vapor equilibria in europium chalcogenide systems.
2. To synthesize single crystals with lower impurity content.

3. To systematically study the effect of trivalent rare earth dopants on Curie temperature.

4. To establish methods for characterizing single crystals with respect to stoichiometry.

5. To clarify the electron transport mechanisms in these magnetic semiconductor systems.

6. To determine the nature of and extent of the glass forming regions in divalent europium systems.

2.0 SYNTHESIS AND CRYSTAL GROWTH OF RARE EARTH CHALCOGENIDES

2.1 Preparation and Characterization of Europium Oxide Crystals

Previous studies[1,2] have described the growth of europous oxide (EuO) single crystals from melts containing excess europium. In this technique a mixture of previously synthesized EuO and Eu-metal, or Eu_2O_3 and Eu-metal, is sealed in tungsten or molybdenum crucibles, heated to 2000-2200°C, and cooled. The growth from metal-rich solutions is necessary because at high temperatures EuO preferentially loses europium into the vapor phase and converts to Eu_3O_4.[3] The partial pressure of Eu over these metal-rich solutions at the melting point of EuO, i.e., 2000°C, is thus sufficient to prevent the Eu loss from the EuO, and single phase crystal can easily be grown. Although crystals have been grown from various metal concentrations, little is known about the details of the liquid-solid-vapor phase relationships between EuO and Eu-metal and what the relationships are between these material parameters and the physical properties. We report the results of our recent work on this system.

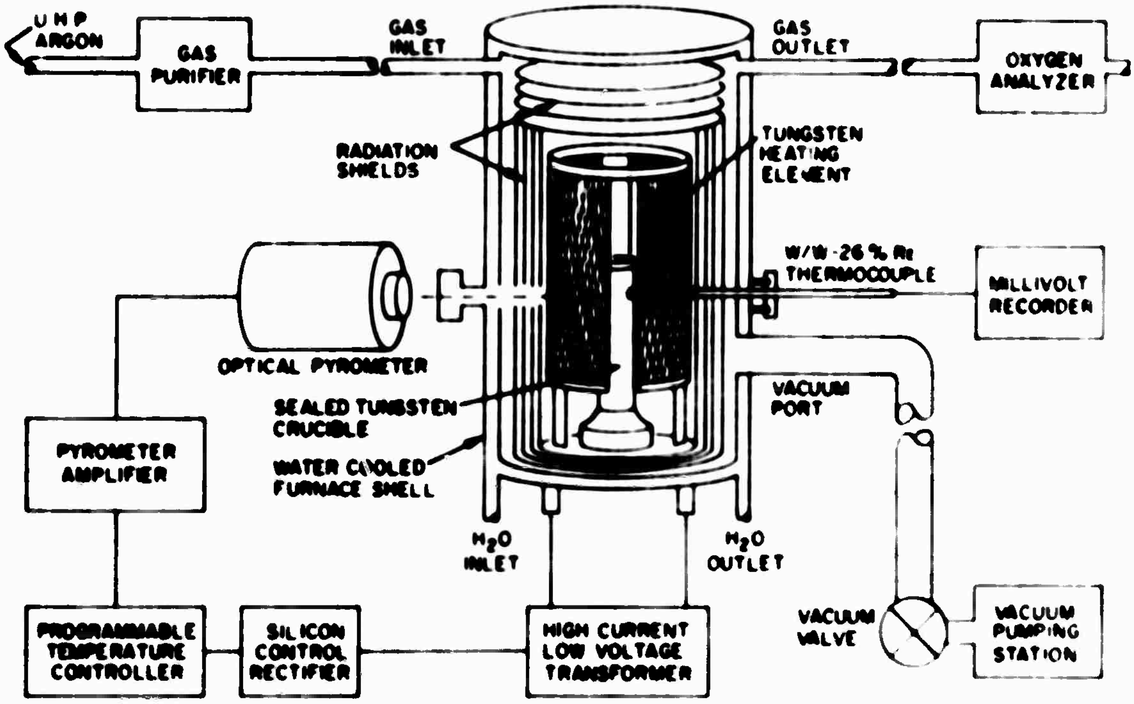

Figure 1. Tungsten Furnace Arrangement

2.1.1 Experimental

The experimental procedure involved the reaction of Eu-metal with Eu_2O_3 or EuO at various temperatures followed by either rapid quenching or slow cooling to room temperature and examination of the resulting charge.[4] Metallographic examination, used to determine the phases present, also proved useful in identifying primary vs. secondary phases. In many cases chemical analyses for total europium content were made and on some samples, particularly those in single crystal form, conductivity measurements as a function of temperature and infrared optical absorption measurements were made.

A tungsten mesh furnace manufactured by Centor was used almost exclusively as the heating source (Figure 1). The tungsten mesh heating element (2" dia. by 4" length) was surrounded by numerous radiation shields and this whole arrangement was enclosed in a gas-tight, water-cooled jacket. The furnace can be operated either in a vacuum or an inert atmosphere, but most of our experiments were done in a flowing atmosphere of high purity argon. Commercially available high-purity argon was further purified and oxygen contents of less than 0.01 ppm, as determined by an in-line analyzer, were normally attained. Such low oxygen content atmospheres are essential to prevent the oxidation of the eating element and radiation shields and prolong their lifetime. In our case we have been operating with the same element and shields for about one year. The temperature was sensed both optically and by a W/W-26%Re thermocouple. The optical sensor and control system consisted of a Barnes photoelectric pyrometer, the output of which was fed into a Leeds & Northrop CAT temperature controller with feedback to a 50 amp silicon controlled rectifier. The output of the thermocouple, the junction of which was located on the crucible containing the charge, was monitored on a separate recorder and in many cases was used for thermal analyses in detecting the heat content differences involved in phase changes. The temperature could be controlled to within ± 0.5°C in the 2000° range with this system.

2.1.2 Results and Discussion

The preliminary results in terms of a phase diagram for the europium-oxygen system are shown in Figure 2. This is a conventional temperature-composition plot which also shows the compositions of the condensed phases in equilibrium with the vapor pressure of pure europium at the temperature indicated (heavy dashed line). This line was determined by heating EuO crystals in Eu-vapor which was in equilibrium with Eu-liquid. Experimentally this was done by containing the EuO crystals in an open crucible which was supported inside a sealed crucible so that the excess Eu-metal in the liquid phase would not be in contact with the crystals. After heating at the proper temperature for about 20 hours the charge was quenched and examined metallographically and then analyzed chemically. It was unneccessary to remove the charge from the tungsten crucible since the crucible is highly insoluble in dilute HCl, while the EuO-Eu melt is highly soluble. From Figure 2 it is evident that Eu-vapor is in equilibrium with a liquid oxide, the composition of which is given on the heavy dashed line, at temperatures above 1350°C. At about 1350° there are three phases, Eu-vapor, liquid oxide of composition X_L, and solid EuO of composition X_S, in equilibrium. Since this defines an invariant point at this pressure, any further lowering of the temperature results in the liquid crystallizing to solid EuO which remains in equilibrium

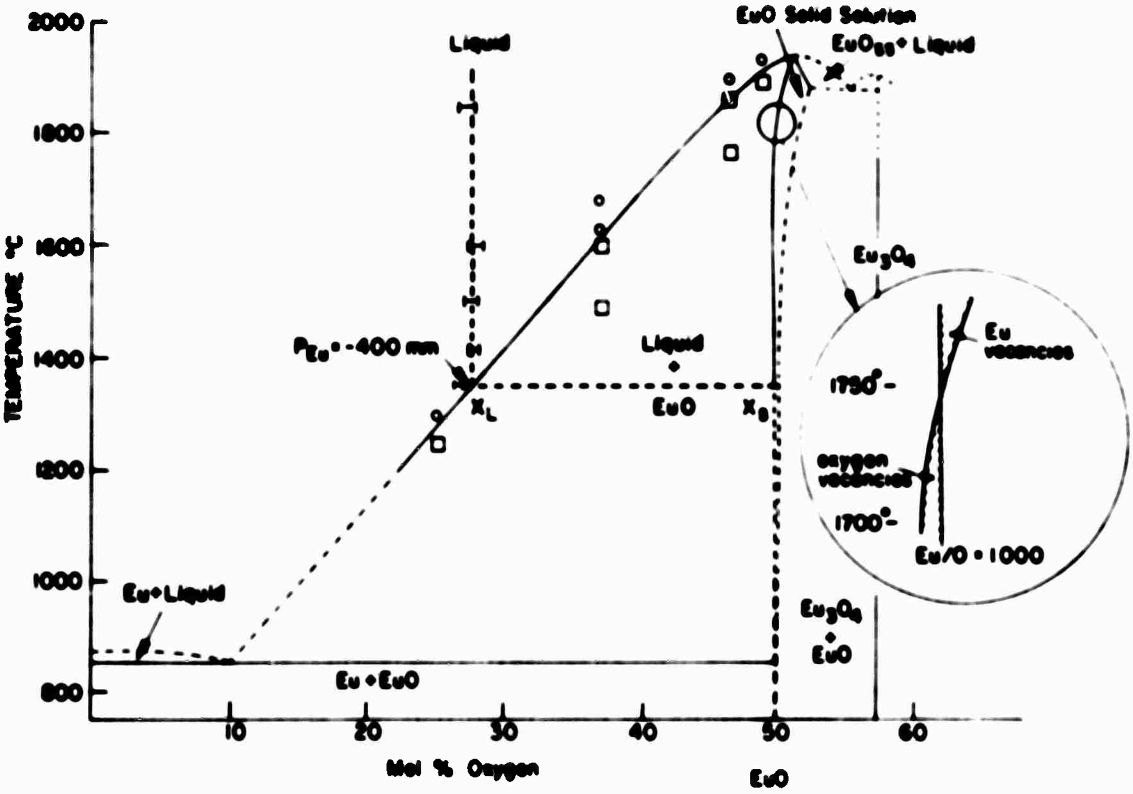

Figure 2: Partial phase diagram of the europium-oxygen system.

with Eu-vapor as the temperature is lowered. The significance of this curve is that it shows that single crystals of EuO can be grown from the liquid phase at much lower temperatures than was thought possible. In fact, we have grown moderate sized crystals at temperatures as low as 1450°C and crystal #89B which showed a sharp metal-insulator transition and on which resistivity and infrared abosrption measurements were made, was grown by cooling from 1650° to 1375°C.

Another important aspect of the diagram shown in Figure 2 is that at high temperatures stoichiometric EuO does not exist. This is shown by the curvature at high temperatures of the phase boundary between EuO and the liquid plus crystal region. The fact that it curves toward the oxygen-rich side i.e., to the oxygen side of a hypothetical vertical line where Eu/O=1.000, means that these compositions contain europium vacancies and trivalent europium. Although the EuO phase is shown to exist over a compositional range in the diagram, the exact extent of this range has not been accurately determined and is thus shown by a dashed line. Our present information indicates it to be no more than a few percent. The important feature, however, is that it presumably narrows at lower temperatures so that some EuO compositions grown at high temperatures with excess oxygen cannot be slowly cooled without the formation of a precipitate of an oxygen-rich phase, i.e., Eu_3O_4. On the other hand, samples grown under the same conditions, but quenched rapidly to room temperature, are single phase EuO containing some trivalent europium compensated by Eu-vacancies. The best evidence for this is from infrared absorption measurements by J. Torrance which show an absorption line associated with Eu^{+++}, as opposed to a high background absorption when an Eu_3O_4-like precipitate is present as a separate phase. The precipitates were also easily monitored by conventional metallographic techniques and the composition confirmed by electron microprobe analyses. Transport measurements on samples prepared according to the phase diagram to have excess oxygen, showed high resistivities and no metal-insulator transitions.

At lower temperatures the phase boundary between EuO and the liquid plus crystal region falls on, and probably crosses, the stoichiometric EuO composition (see insert in Figure 2). Samples prepared in this region, particularly those on the Eu side of EuO, presumably have oxygen vacancies which are responsible for their metal insulator transitions and multiple absorption bands in the far infrared. The width of the EuO field at these temperatures is very narrow, i.e., probably less than 0.5%, and cannot be easily determined by conventional analytical techniques. A complicating factor in determining the width of a compositional field this small by chemical methods is the high background impurity level of most europium compounds, which may be many thousand PPMA. From the transport and the infrared measurements and metallographic examinations, however, it can be concluded that the shape of the EuO field as a function of temperature must be very similar to that shown in Figure 2. The important feature is that the boundary crosses the stoichiometric EuO composition, and we believe that compositions on the Eu side have oxygen vacancies while those on the oxygen side have Eu-vacancies. Further, it appears that in the temperature range of 1700-1800°C, the boundary curve falls on top of the vertical stoichiometric EuO line and any crystals grown with excess metal in this temperature range would have an europium-to-oxygen ratio very close to one.

The validity of this diagram has been checked by growing crystals from compositions containing different Eu-concentrations and by cooling and quenching from different temperatures. From these experiments reproducible results consistent with the diagram have been obtained. The congruent melting point of EuO is 1980 ± 10°C, lower than had been previously reported,[2] and the minimum temperature at which liquid oxide can be in equilibrium with crystalline EuO under the vapor pressure of Eu-metal is 1350°C. The pressure at this temperature is $\sim$ 400 mm Hg.

The shape of the liquidus curve for the high Eu-metal concentrations and the eutectic composition between Eu and EuO is still uncertain (dashed lines). There is some evidence from quenching experiments that two immiscible liquids, liquid metal and liquid oxide, are formed between 3 and 15 mole% oxygen. Within experimental error (± 3°C), thermal analyses showed that the freezing point of Eu-metal was not lowered by the addition of EuO, which means that the eutectic temperature is roughly 860°C, the melting point of the metal.

2.2 EuS Preparation and Characterization

Previous studies have contributed much to elucidate the relationship between the magnetization and the conductivity of the divalent europium chalcogenides. But, despite the fact that the conductivity is strongly dependent on the composition and purity of the samples, little has been done to understand the details of this dependence. It is rather well established that the stoichiometry of these compounds, as well as the number and type of impurities present, are the two materials parameters which are primarily responsible for conductivity variations between samples. The question of stoichiometry, i.e., the Eu/S ratio, and its effect is a complex one and can only be completely understood if the background impurity level is lowered to a

TABLE I

Solid State Mass Spectrometric Analyses of Eu Metal and Eu_2O_3*

Element	Eu Metal A 99.9	Eu Metal B 99.95	Eu_2O_3 A 99.995	Eu_2O_3 B 99.999
Ta	3			
Lu	10			
Yb	20			
Tm	<30			
Ho, Dy, Tb, Gd	<30	120		
Sm	10			
Nd	<10			
Ce	<10			
La	<10			
Ba	10			
Cs	10-100			
Ir	<10	10		
Y	20			
Sr	<10	50		
C	100	300	1600	200
Zn	300	300		
O	1400	1000		
Mn	300	100		
Fe	30	30	10	10
Cr	<10			
Ti	<10			
Sc	<10			
Ca	200	100	60	60
K	10	20	50	200
Cl	2000	300	<10	<10
S	500			
Si	500	100	<10	100
Al	10	10	<30	<30
Mg	3000	300	100	<30
Na	10	50	18	<100
Se				
Ga		20		
Cu			20	<2
N		50		60

* Impurity concentration in ppm atomic

degree where its contribution to the conductivity is not significant. This study is concerned with lowering the total impurity content so that the effects of stoichiometric variations can be studied.

The origin of impurities in europium compounds is mainly from the europium or the europium salt used as the source material. The listed purity of the purest commercially available europium salts ranges from 99.95 for Eu-metal to 99.999 for Eu_2O_3. However, these results are usually derived from emission spectrographic analyses and the lighter elements such as H_2, C, N, etc., are not reported. Table I shows the results of our analyses of two 3-9's Eu-metal samples and two typical 5-9's Eu_2O_3 samples by the Solid State Mass Spectrometer. It is seen that if the lighter elements are included, the total impurity concentration is generally higher than that claimed by the manufacturers. Further, although the overall impurity level is high, particularly when compared to the more conventional semiconductors, it is significantly lower in the sesquioxide than in the metal. For this reason, and because of the extreme difficulty in removing impurities from the metal, it was felt that the overall impurity level in EuS would be lower if Eu_2O_3 rather than Eu-metal were used as the europium source material. The problem then was, how effectively can the oxygen be removed from Eu_2O_3 in the formation of EuS?

Domage, et al.,[5] first showed that europium sulfide is readily formed by heating the sesquioxide, Eu_2O_3, in H_2S gas at 900°C, the reaction being:

$$2\,Eu_2O_3 + 6H_2S \qquad\qquad 4EuS + 6H_2O + S_2. \qquad (1)$$

Although their EuS was shown by chemical analyses to contain the theoretical amount of Eu (and S), no analyses were made to determine trace quantities of impurities such as oxygen. We have now studied the H_2S-Eu_2O_3 reaction as a function of temperature (300°-1800°C) and determined the phase relationships as well as the oxygen content.

2.2.1 Experimental

The H_2S-Eu_2O_3 reactions were carried out by passing H_2S gas through a horizontal silica glass tube in which a boat containing the Eu_2O_3 sample was placed. For reactions up to 1250°C a platinum container was used and this was heated with a kantnal resistance furnace. Above 1250°C a vitreous carbon boat lined with partially sintered EuS was used. This prevented sample contact with the container and minimized any reaction with the carbon. At these high temperatures RF heating was used, with a carbon susceptor inside the gas-tight silica tube. Temperatures as high as 2000°C were attainable by this arrangement. In both heating arrangements the samples could be cooled to room temperature in a matter of minutes, either in H_2S or an inert gas. The H_2S gas contained less than 50 ppm impurities, the major one being H_2O. The reaction times varied from several days at low temperatures to several hours in the 1800°C range. After reaction the samples were quenched and the phases identified by conventional x-ray diffraction techniques. In certain cases magnetic susceptibility measurements were used to further characterize the phases. The oxygen was determined by neutron activation analyses at the Sterling Forest Laboratory of Union Carbide. The total impurity content was obtained by an AEI MS-7 spark source mass spectrograph.

In many cases, the powders prepared in the above manner were converted into single crystals by sealing in tungsten crucibles and cooling from 2490°C.[2,6] The optical absorption measurements on the single crystals were done at room temperature on a Carey model 14 spectrometer.

2.2.2 Results and Discussion

The hydrogen sulfide dissociation reaction

$$2H_2S_{(g)} \qquad 2H_{2(g)} + S_{2(g)} \tag{2}$$

has been studied in considerable detail and the degree of dissociation, α, as a function of temperature is well known.[7] Knowing α, the partial pressures of H_2S, H_2, and S_2 can easily be obtained and the equilibrium constant K_p for reaction (2) is given by:

$$K_p = \frac{\alpha^3 P}{(2+\alpha)(1-\alpha)^2}, \tag{3}$$

where P is the total equilibrium pressure. Since large excesses of $H_2S_{(g)}$ have been used in the reaction, it can be assumed that the Eu_2O_3 and EuS will only slightly effect its dissociation. Thus, the partial pressures of H_2S and S_2 from the H_2S dissociation (reaction (2)) can be substituted into the expression for the equilibrium constant for reaction (1). Thus

$$K_{p_{EuS}} = \frac{P^6_{H_2O}\, P_{S_2}}{P^6_{H_2S}}, \tag{4}$$

and $K_{p_{EuS}}$ can be calculated assuming $P_{H_2O} = 1 - (P_{H_2S} + P_{S_2})$. From this the

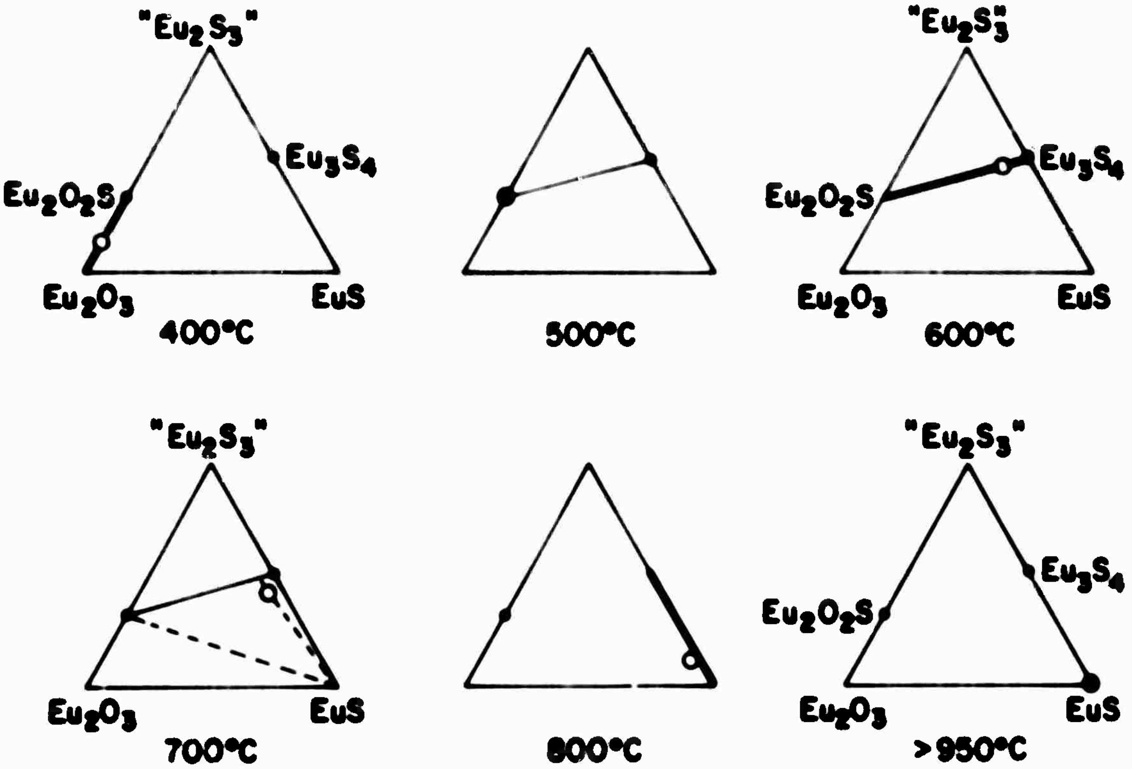

Figure 3: Isothermal sections showing the phases present in the Eu_2O_3 - "Eu_2S_3" - EuS system. Open circle shows the composition at the temperature indicated.

following values for $K_{p_{EuS}}$ were obtained:

TABLE II

Equilibrium Constant, K_p,
at Various Temperatures for Equation (1)

T (°C)	K_p
750	1.04×10^{-9}
800	1.02×10^{-8}
850	6.3×10^{-8}
900	4.9×10^{-7}
1050	6.66×10^{-5}
1150	1.64×10^{-3}
1200	1.05×10^{-2}

From the slope of the straight line in the 1/T vs. Log $K_{p_{EuS}}$ plot, a value of $\Delta H = 58{,}000$ Cal for reaction (1) is obtained.

The equilibrium phases formed at the various temperatures are shown in Figure 3 in terms of the ternary system Eu_2O_3-Eu_2S_3-EuS. The composition, at the temperatures indicated, is shown by the open circle. It is seen that below about 400°, the sesquioxide Eu_2O_3 is the principle phase. Since the reaction rates at these low temperatures are extremely slow, it is unlikely that true chemical equilibrium has been reached in these experiments. However, the fact that Eu_2O_3 still remains after "reacting" for several hundred hours, is sufficient justification for the diagram to be constructed as it is.

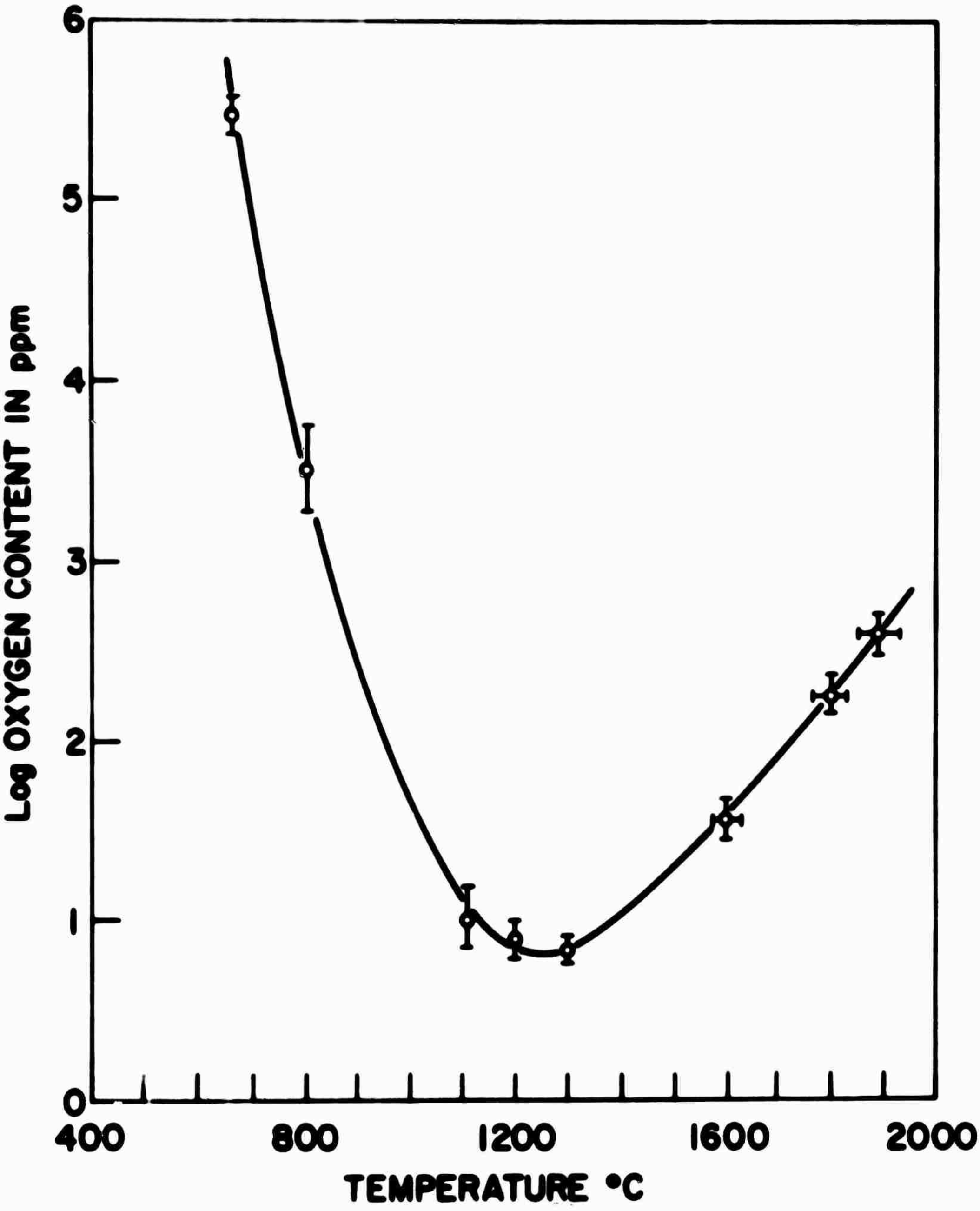

Figure 4: Oxygen content in europium sulfides after the H_2S - Eu_2O_3 reaction.

Between 400° and 550°C the Eu_2O_3 is converted to the oxysulfide Eu_2O_2S, a hexagonal compound with a = 3.86 Å and c = 6.702 Å, in which the europium is still trivalent. Eu_3S_4 can be detected at 575°C and it is in equilibrium with Eu_2O_2S between 575° and about 650°C. There is no evidence for the existence of Eu_2O_2S above 650°C, at which temperature Eu_3S_4 is the major phase containing traces of EuS. Even at 700°C, where Eu_2O_2S is no longer present as a distinct phase and where Eu_3S_4 and EuS are in equilibrium, there is still a considerable amount of oxygen present. This is shown by the composition (open circle) at this temperature being off the "Eu_2S_3"-EuS join and by the results of the oxygen analyses shown in Figure 4. As the temperature is increased, the Eu_3S_4 phase is converted to EuS and the total oxygen content becomes smaller. EuS is the only detectable phase above 900°C, and its oxygen content reaches a minimum at about 1300°C. There is evidence from previous microstructure studies[8] and Mössbauer[9] measurements that EuS can contain up to several percent trivalent europium in solid solution. It would be expected that this solubility would perhaps be a maximum at about 800°-900°C where the Eu_3O_4 phase is in equilibrium with EuS. Precision lattice constant measurements did show a slight difference between the 800° samples and those prepared at higher temperatures - see Table III. It is probable that this difference is due to trivalent europium in the EuO lattice at the low temperatures.

TABLE III.

Lattice Constant of EuS

Preparation Temperatures	Lattice Constant (Å)
800°C	5.965 ± .001
1200°C	5.967 ± .001
1600°C	5.966 ± .001
1800°C	5.967 ± .001
2000°C	5.968 ± .001

It is seen from Figure 3 that an oxygen content as low as 50-75 ppm is achieved for samples reacted at 1200°-1300°C. This represents the total oxygen found in a powdered sample, and represents an upper limit for oxygen in the lattice since no special precautions were taken to prevent surface absorption from the atmosphere. It is not completely clear why an increase in oxygen content occurs in those samples heated above 1300°C, but the most plausible explanation is that at these higher temperatures there is an increasing tendency for the EuS to sinter to a high density on the surface where it is formed by the reaction with H_2S. This high density coating then prevents the inner core of Eu_2O_3 from reacting with the gas phase. In fact, when pressed pellets of Eu_2O_3 were reacted at 1850°C for 16 hours, a sharp boundary between the dense black EuS coating and the white oxide core could easily be observed by normal metallographic techniques. By measuring the thickness of this EuS coating as a function of time, a reaction rate of roughly 0.08-0.1 mm/hr. at 1850°C was obtained. At lower temperatures, i.e., 1000-1300°C range where there is less grain growth of the EuS and it is much more porous, the boundary became diffuse and the reaction rate increased. Thus, it is likely that at high temperatures some unreacted Eu_2O_3 is present which is the source of the increased oxygen content.

Considerable differences in melting temperatures and crystal growth were observed in a series of samples grown from powders containing different oxygen concentrations. Those with the lowest concentration had higher melting points and grew larger and more perfect crystals than those which analyses showed to contain several thousand ppm oxygen. The optical absorption coefficients of the low-oxygen crystals were in general also lower, but since the sulfur:europium ratio is a critical parameter in determining the absorption, this may not be too significant.

2.3 Metallic Rare Earth Monosulfides and the $Eu_{1-x}Gd_xS$ System

The synthesis of trivalent metallic rare earth monosulfides has been previously described[10,11,12] but there is little information on the growth of single crystals of these compounds. The monosulfides all melt above 2000°C and crystallize with the NaCl-type structure. During studies of solid solutions of the insulating divalent europium sulfides and trivalent metallic monosulfides, it became apparent that it was necessary to characterize the latter materials with respect to their transport and magnetic properties. GdS had been selected as a dopant for EuS because, like Eu^{++}, it has a half filled 4f shell and avoids the complication of an orbital contribution to the magnetic moment. It also provides a means of studying a solid solution system such as $Eu_{1-x}Gd_xS$ in which the number of spins is constant for all values of x.

Three compounds GdS, LaS and YS were selected for a study of transport properties. As with GdS, LaS and YS crystallize in the NaCl-type

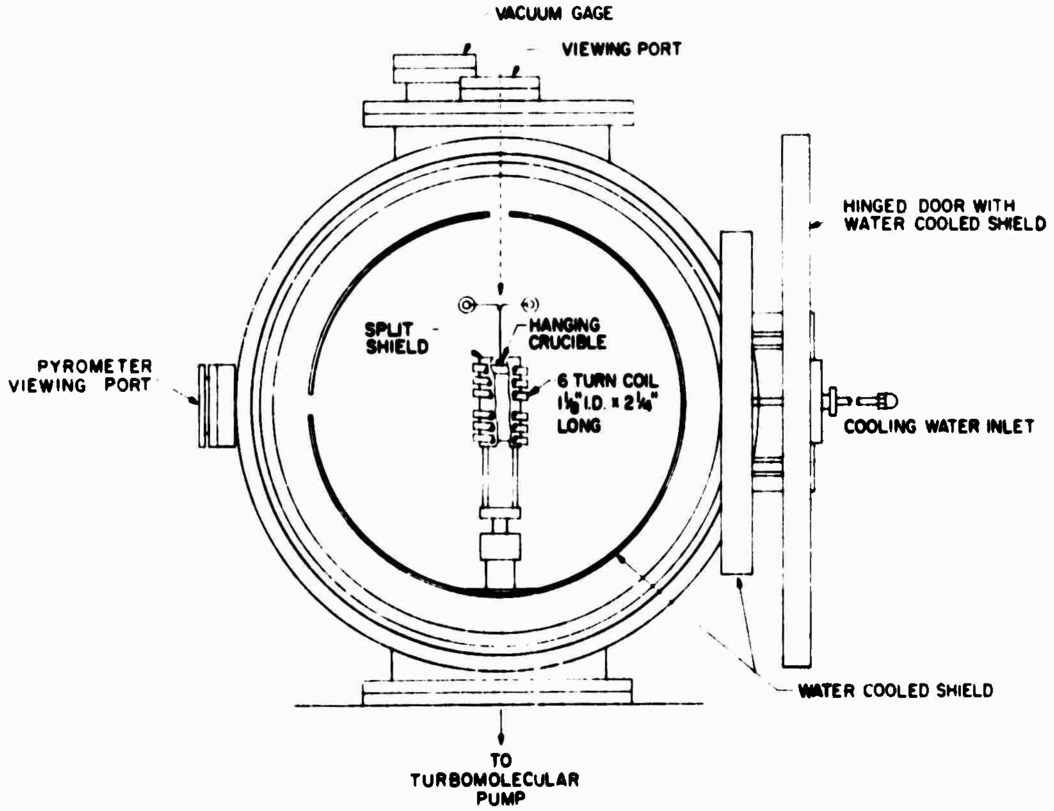

Figure 5: High Temperature Vacuum RF Furnace

structure and the compounds are isoelectronic and therefore should have the same conduction electron concentration. La^{+++} and Y^{+++} have no 4f electrons and thus no magnetic moment and their radii bracket that of Gd^{+++} so that their sulfides provide the requisite compounds for a comparative study of transport properties.

2.3.1 Synthesis and Crystal Growth of GdS, LaS and YS

The simplest and most direct synthesis of metallic rare earth sulfides involves the vapor transport of sulfur from one quartz chamber to a second chamber containing the rare earth metal.[11,12] In the reported procedures, reactants have been heated to ∿ 1000°C in quartz in order to obtain homogeneous samples. We have found that the quartz is attacked in the temperature range 700-1000°C and have limited the temperature to 600°C in this first stage of the synthesis. This material is then transferred to a tungsten crucible for homogenization at 1800°C. With this procedure it is not necessary to reduce the rare earth metal to fine filings for the first stage of reaction and bulk metal is used to reduce handling and contamination.

Crystals were grown in an induction heated RF furnace (Figure 5) using a 10^{-6} torr vacuum to protect the crucible from surface reaction. A split tantalum shield surrounding the crucible reduces gradients and the crucible, suspended from a fine Ta wire, is positioned to adjust the temperature profile along its length. Temperature measurement and control was achieved with an L&N automatic optical pyrometer, surface temperature having been calibrated with a black body measurement obtained with the same geometry. Pressed pellets of the homogenized powders were sealed by electron beam welding in 3/8" x 2" tungsten crucibles and heated to 2400°C, then slowly cooled to room temperature.

2.3.2 Results

The resulting ingots of GdS, LaS and YS were gold-colored metallic cylinders which showed no evidence of reaction with the tungsten crucibles. The samples cleaved parallel to (100) planes as cleanly as the insulating chalcogenides. Lattice constants shown in Table IV were obtained with a Guinier x-ray focussing camera using Si as an internal standard. The lattice constants are the same as those reported by Iandelli.[13]

TABLE IV.

Lattice Constants of Metallic Rare Earth Monosulfides

	a_0 (Å)
GdS	5.566 ± .001
LaS	5.854 ± .001
YS	5.496 ± .001

2.3.3 The $Eu_{1-x}Gd_xS$ Solid Solution System

It became apparent from initial attempts to prepare compositions in the solid solution system $Eu_{1-x}Gd_xS$ that a single sub-solidus firing would not produce homogenous samples. Repeated firing with grinding would be costly in crucible materials and expose the materials to contamination. We therefore decided to melt the samples, accept chemical gradients and determine whether sufficiently large homogeneous regions could be found for analysis. Using the same procedure described for the metal samples, appropriate mixtures of EuS and

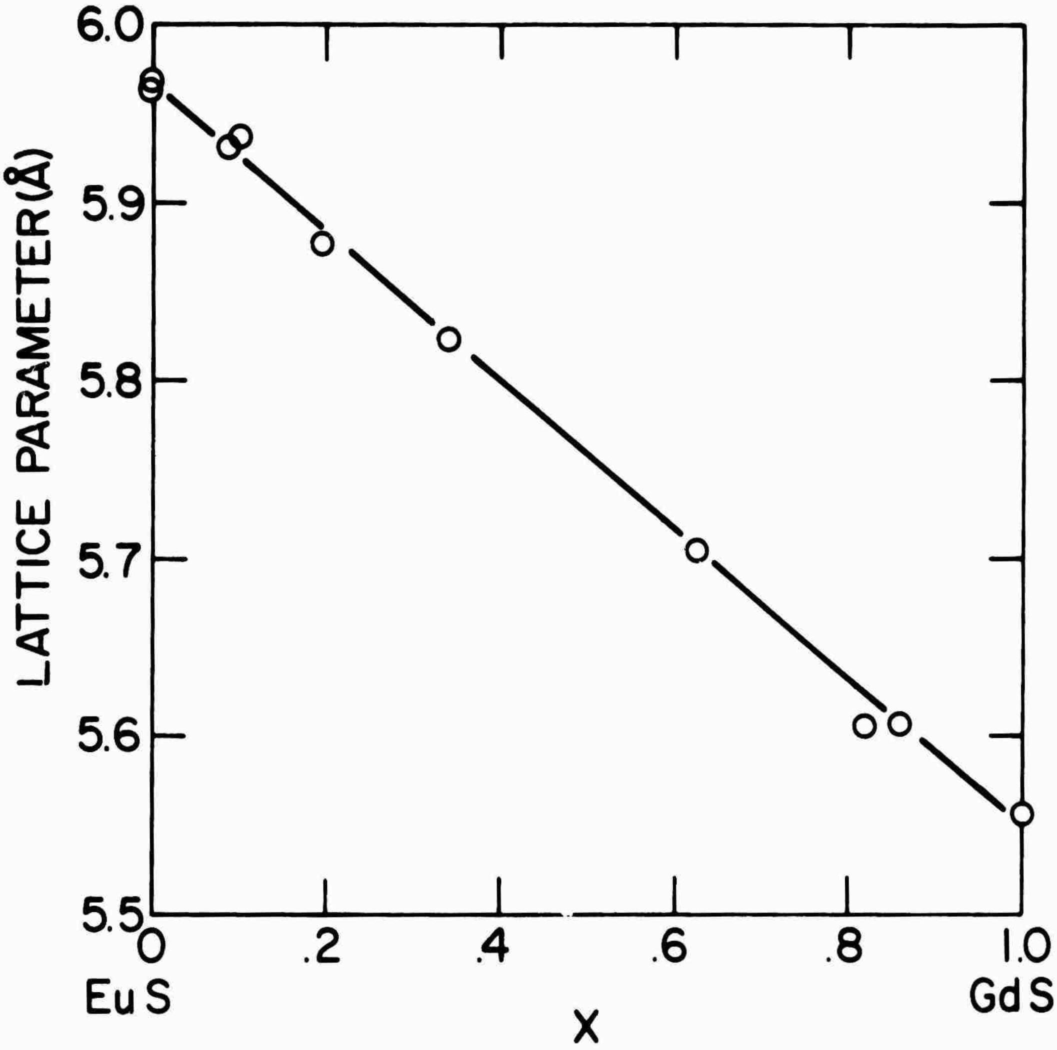

Figure 6: Lattice parameter for face centered cubic EuS-GdS solid solution system.

GdS were heated to melting and slowly cooled. The resulting ingot was sectioned and the microprobe was used to map out regions of homogeneity. It was found possible to select sufficiently large homogeneous regions for x-ray and magnetic measurements. Using this technique a single ingot provided a range of concentrations for analysis.

X-ray analysis shows that the NaCl-type structure is maintained over the entire composition range x = 0 to 1 in $Eu_{1-x}Gd_xS$. The linear dependence of lattice parameter vs. composition is shown in Figure 6.

2.4 Vaporization Studies of EuS and EuSe

It is evident from the results of optical, magnetic and transport measurements that the divalent Eu chalcogenides all exist over a range of concentrations. The dependence of Eu concentration on pressure has been discussed for EuO in section 2.1. Since it is possible to adjust the Eu concentration and therefore the vacancy concentration in EuS and EuSe by quenching from different temperatures during crystal growth, or by annealing and quenching techniques, a study of the vapor-solid equilibria in these systems was undertaken. The data were obtained with a computer controlled mass spectrometer designed for high temperature Knudsen effusion measurements.[14] The solids EuS(s) and EuSe(s), unlike the oxide, are in equilibrium with gaseous EuS(g), Eu(g), S(g) and S_2(g) and EuSe(g), Eu(g), Se(g), and Se_2(g), respectively. Table V lists the heats of vaporization associated with the reactions shown in equations 5 and 7 and the heats of dissociation associated with reactions 6 and 8.

TABLE V.

Heats of Vaporization and Dissociation for EuS and EuSe

Reaction	ΔH kcal/mole	Temperature Range
5) $EuS(s) \rightleftharpoons EuS(g)$	123	1730-2052°K
6) $EuS(g) \rightleftharpoons Eu(g) + S(g)$	94	1730-2052°K
7) $EuSe(s) \rightleftharpoons EuSe(g)$	122	1550-1927°K
8) $EuSe(g) \rightleftharpoons Eu(g) + Se(g)$	74	1550-1927°K

2.5 Divalent Europium Glasses

The high Faraday rotations associated with the divalent europium ion can be used in magnetooptical devices. Consequently, the ability to substitute varying amounts of the Eu^{++} ion into a stable, readily formable matrix such as a glass, has considerable merit. We had previously investigated a number of glass forming systems which would incorporate the Eu^{++} ion and reported on the EuO-B_2O_3-Al_2O_3 system[15] where a large glass-forming region, up to 43 mole % EuO, was shown to exist. We are currently studying this system in more detail to see if it is possible to extend the region to include more Eu^{++} where there would be a possibility of magnetic order.

By using improved quenching techniques we were able to increase the total Eu concentration in the stable glass phase from 43 to 58%. However, at the higher Eu concentrations roughly 10% of the Eu went into the glass as trivalent. These glasses, therefore, must now be defined in terms of the quaternary system EuO-RE_2O_3-B_2O_3-Al_2O_3, where RE is a trivalent rare earth. The glasses are not restricted to Eu^{+3} because it is possible to eliminate most of the Eu^{+3} by the substitution of other trivalent rare earths. The addition of 5% Gd_2O_3 to the glass melt lowered the Eu^{+3} concentration by $\sim$ 5%, with the Eu^{+2} concentration remaining constant.

Susceptibility measurements on the highest Eu^{+2} content glasses showed no evidence of magnetic order at helium temperature. Several experiments were carried out where the glass was annealed in Eu vapor at high temperatures in an attempt to produce some conductivity and perhaps enhance the Eu-Eu exchange interactions. These experiments have not been successful because the glasses devitrified into several crystalline phases. The annealing experiments will be continued at lower temperatures and some glass melts will be made in closed crucibles containing a positive Eu-pressure.

3.0 PHYSICAL PROPERTIES

3.1 Magnetic Ordering of $Eu_{1-x}Gd_xS$

In a continuing investigation[16,17] of europium-gadolinium chalcogenides we have recently studied in detail the magnetic properties of the $Eu_{1-x}Gd_xS$ solid solution system. This system has several unique properties which make it important from both a theoretical and practical viewpoint. The compounds have the face centered cubic structure and form a continuous series of solid solutions from $x = 0$ to 1. Both europium and gadolinium in this structure have a spin-only moment ($S = \frac{7}{2}$) which is well localized in the ion 4f shell. The above characteristic simplifies theoretical work.

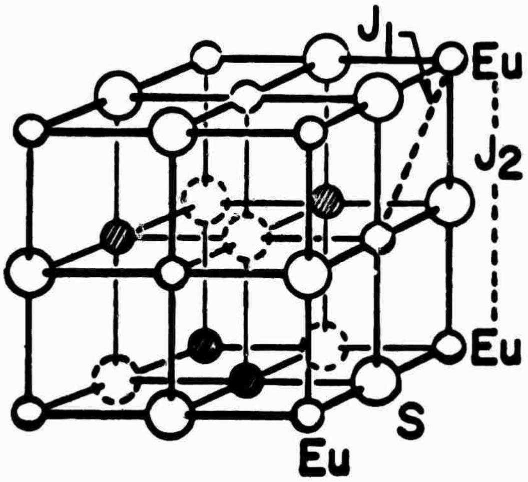

EuS

Figure 7: EuS crystal structure showing the nearest neighbor exchange (J_1) and the next nearest neighbor exchange (J_2).

One of the important features in $Eu_{1-x}Gd_xS$ is the valance differece of the two rare earth ions: europium is divalent (Eu^{2+}) and gadolinium is trivalent (Gd^{3+}). Since the anion is divalent sulfur (S^{2-}), EuS is an ionic insulator. GdS, however, is metallic because each Gd atom contributes an extra electron. A striking effect caused by this change in electron concentration is the large change in the magnetic transition temperature. The Curie temperature (T_c) of ferromagnetic EuS can be raised by a factor of three with a few percent addition of gadolinium. This allows the magnetic exchange interactions via conduction electrons to be studied in a detailed manner.

3.1.1 Magnetic Properties:

The starting material, EuS, is ferromagnetic[18] with a T_c of 16.5°K and a magnetic moment of 212 emu/gm. This moment corresponds to 7 unpaired spins in the europium 4f shell with all Eu ion moments aligned parallel. As shown in Figure 7, the magnetic ions are at crystallographically equivalent lattice sites, in this case in the center of a sulfur octahedron. Two exchange interactions have been established in EuS; the strongest is a nearest neighbor exchange (J_1, Figure 7) which is positive and a next nearest neighbor interaction (J_2) which is negative. In the europium chalcogenides J_1 appears to be a strong function of interatomic spacing while J_2 is due to superexchange and is less sensitive to lattice parameter. In EuS, J_1 is about 6 times more effective than J_2.

The other end member of the solid solution series, GdS, is known to be antiferromagnetic[19] with a transition temperature of 60°K. In constrast to EuS, GdS has a strong negative J_1. J_2, however, remains negative. Thus solid

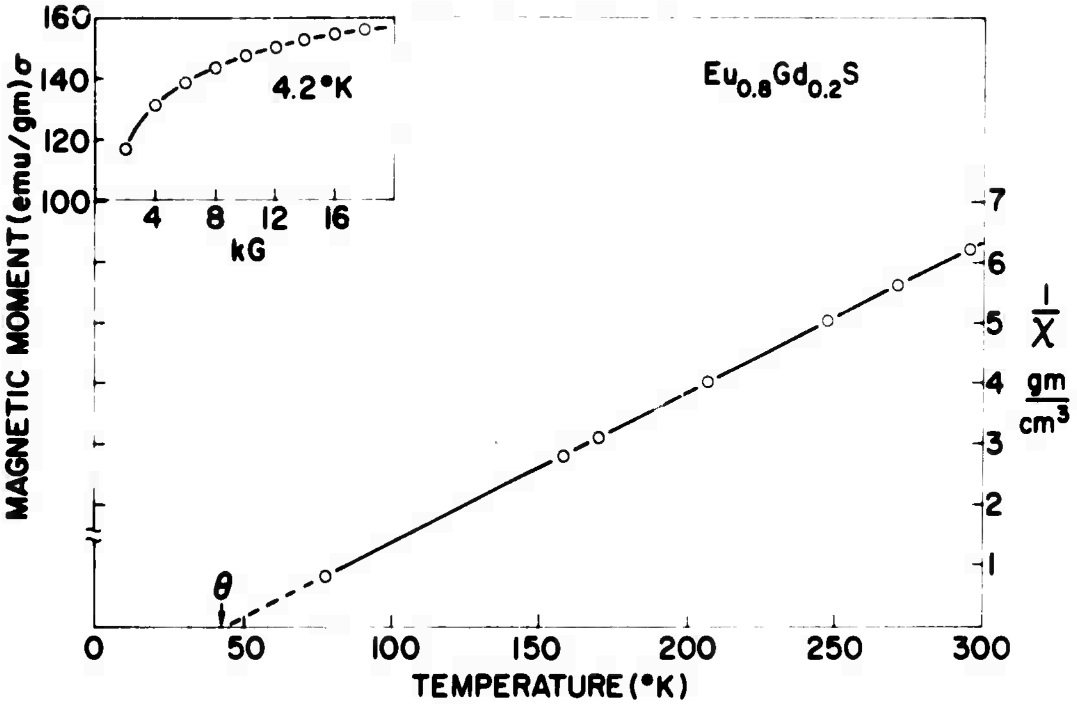

Figure 8: Magnetic moment and reciprocal susceptibility of $Eu_{.8}Gd_{.2}S$.

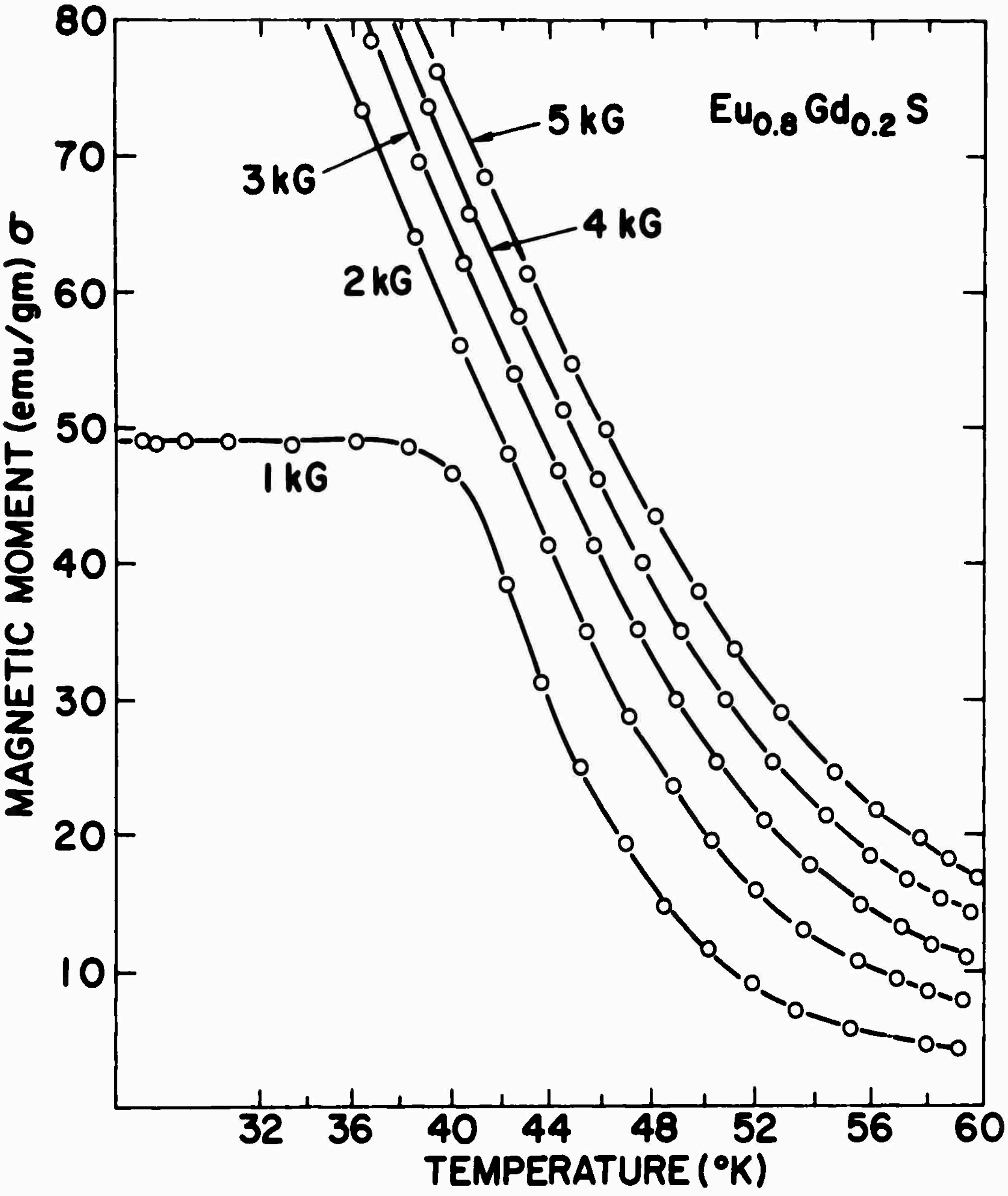

Figure 9: Magnetic moment of $Eu_{.8}Gd_{.2}S$ vs. temperature in the vicinity of the Curie temperature.

solutions of EuS and GdS bring together the complex combination of an electrically insulating ferromagnet with a metallic antiferromagnet.

The magnetic properties of $Eu_{1-x}Gd_xS$ are given in Figures 8 through Figure 14. A typical set of magnetic measurements is shown in Figure 8. For this example we choose $Eu_{.8}Gd_{.2}S$ having $T_c = 44.7K$. The paramagnetic region is plotted as $1/\chi$ vs. T. This straight line plot means that a Curie-Weiss law is followed:

$$\chi = \frac{C}{T-\theta} \tag{9}$$

where χ is the magnetic susceptibility, C is the Curie constant, T the temperature, and $\theta = 45°K$ marks the intercept of $\frac{1}{\chi}$ on the temperature axis. Simple theories[18] give θ as the sum of the exchange interactions found in the material: for a ferromagnet, θ is approximately equal or slightly larger than T_c.

Below T_c we are in the region of spontaneous moment, i.e. the ferromagnetic state. From the shape of the magnetization curves in the region of T_c (Figure 9) an accurate value for T_c can be determined. This is done by using the relation[20]

$$a(T-T_c)\,\sigma + bT\sigma^3 = H \tag{10}$$

where a and b are constants and σ is the measured moment at temperature T in field H. The above expression can be obtained from the thermodynamic free energy or the expansion of the Brillouin function. Plotting a series of curves σ^2 vs. H/σ as indicated in Figure 10 allows the value of T_c to be obtained from the isotherm intercepting the origin ($T_c = 44.7K$).

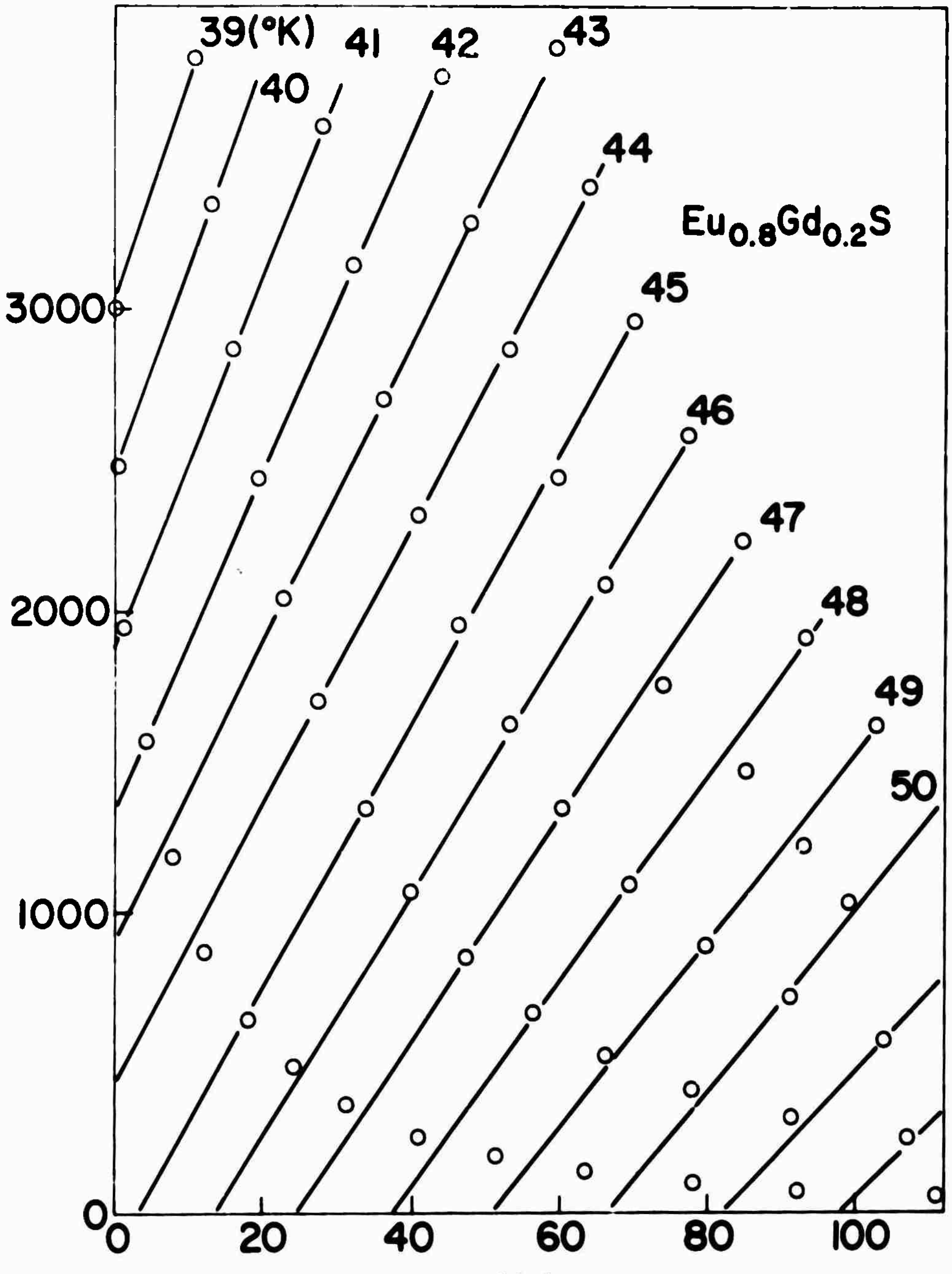

Figure 10: Plot of σ^2 vs. H/σ for data shown in Figure 9.

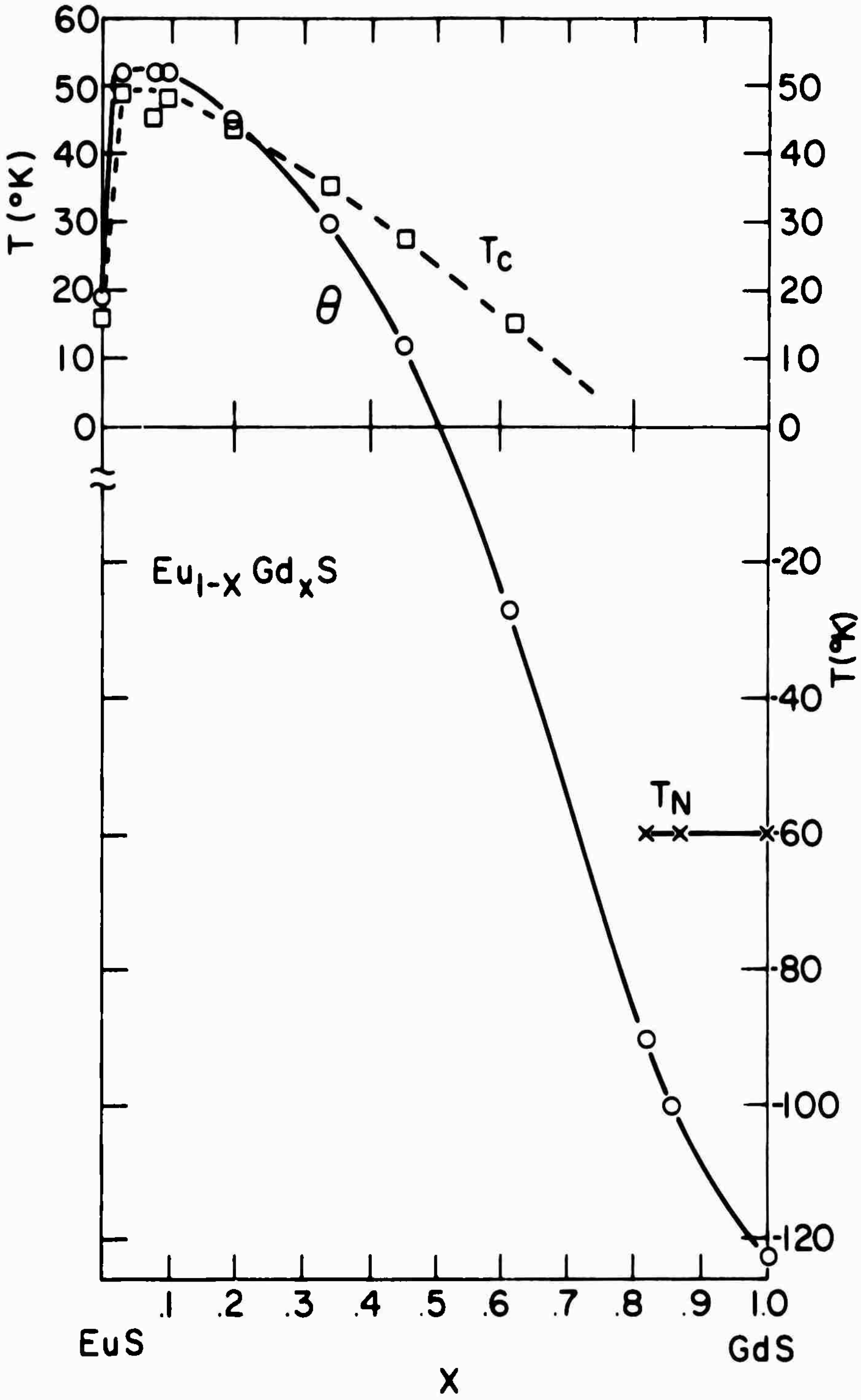

Figure 11: θ and T_c as a function of x for $Eu_{1-x}Gd_xS$.

The values for θ and T_c obtained from magnetic moment and susceptibility measurements, as just discussed, are plotted in Figure 11. First note the sharp increase in T_c and θ that occurs when only a few percent Gd are added. This can be interpreted as a strong increase in J_1 caused by an indirect exchange through the conduction electrons that are now present. For compositions from x = 0.03 to 0.2, both T_c and θ remain about the same, indicating that the average exchange interaction is constant in this range. At values of gadolinium concentration from x = .2 to .6, θ drops significantly below the Curie temperature and for $x > .5$, θ becomes negative. This composition region reveals clearly the complexity of the magnetic properties. For compositions above x = .8 a normal antiferromagnetic behavior is observed.

With the observed complex behavior of this system, a problem arises as to the proper value to choose for the zero field magnetic moment (σ_0). The values shown in Figure 12 are obtained from the magnetization curves plotted in Figure 13. We have analyzed the σ vs. H curves with an empirical equation of the form[20]

$$\sigma = \sigma_0 \left(1 - \frac{a}{H}\right) + \chi_0 H; \qquad (11)$$

where a and χ_0 are constants fitted to the data. Because of the $\frac{a}{H}$ term, the expression cannot be used in the demagnetization region below 10kG. The $\frac{a}{H}$ term takes account of everything that prevents magnetic saturation, such as anisotropy, imperfections and domain effects. In the high field region, 20 to 100 kG, the second term χH represents rotation of the ion moments against exchange forces as will be described in section 3.1.3. The tabulated data shown in Table VI, including σ_0 in Figure 12, were obtained by a least squares fit of the curves in Figure 13.

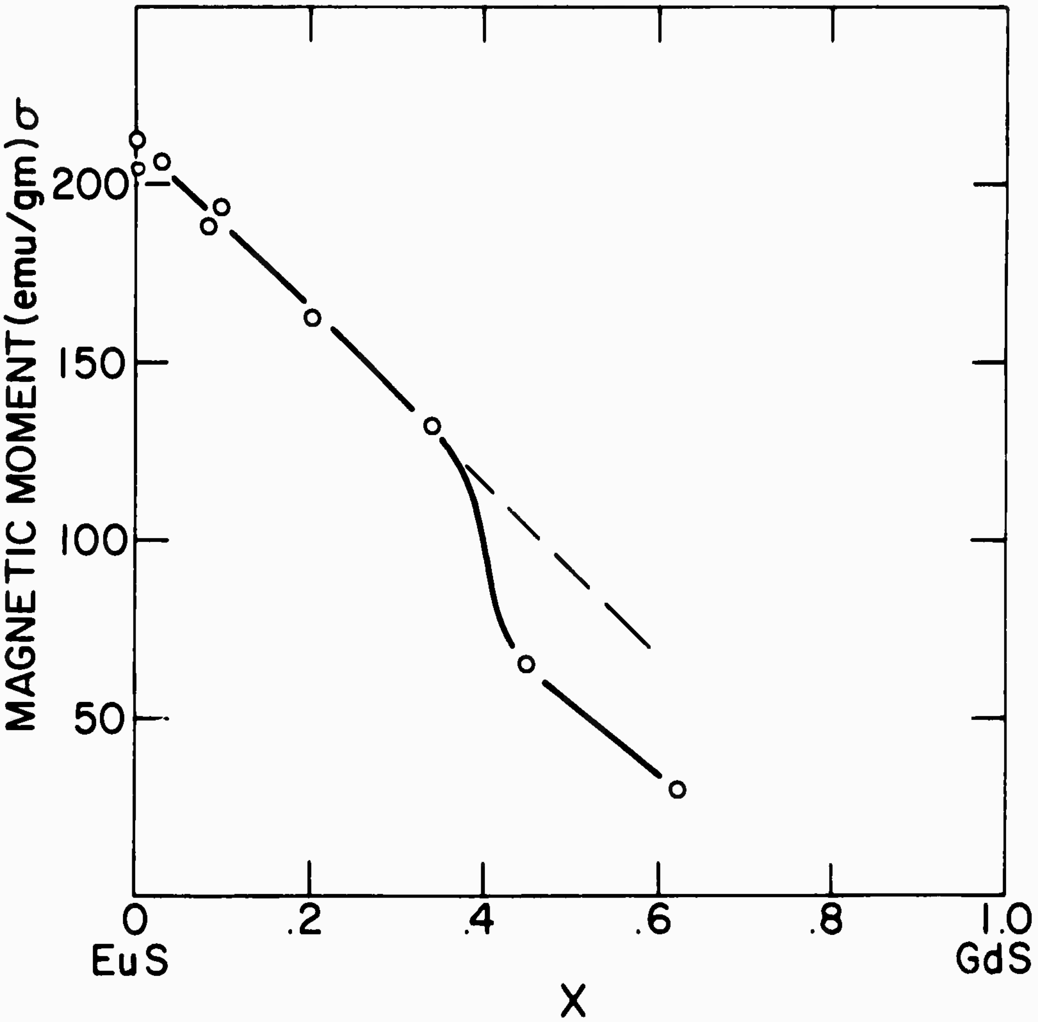

Figure 12: Saturation magnetic moment of $Eu_{1-x}Gd_xS$ as a function of composition.

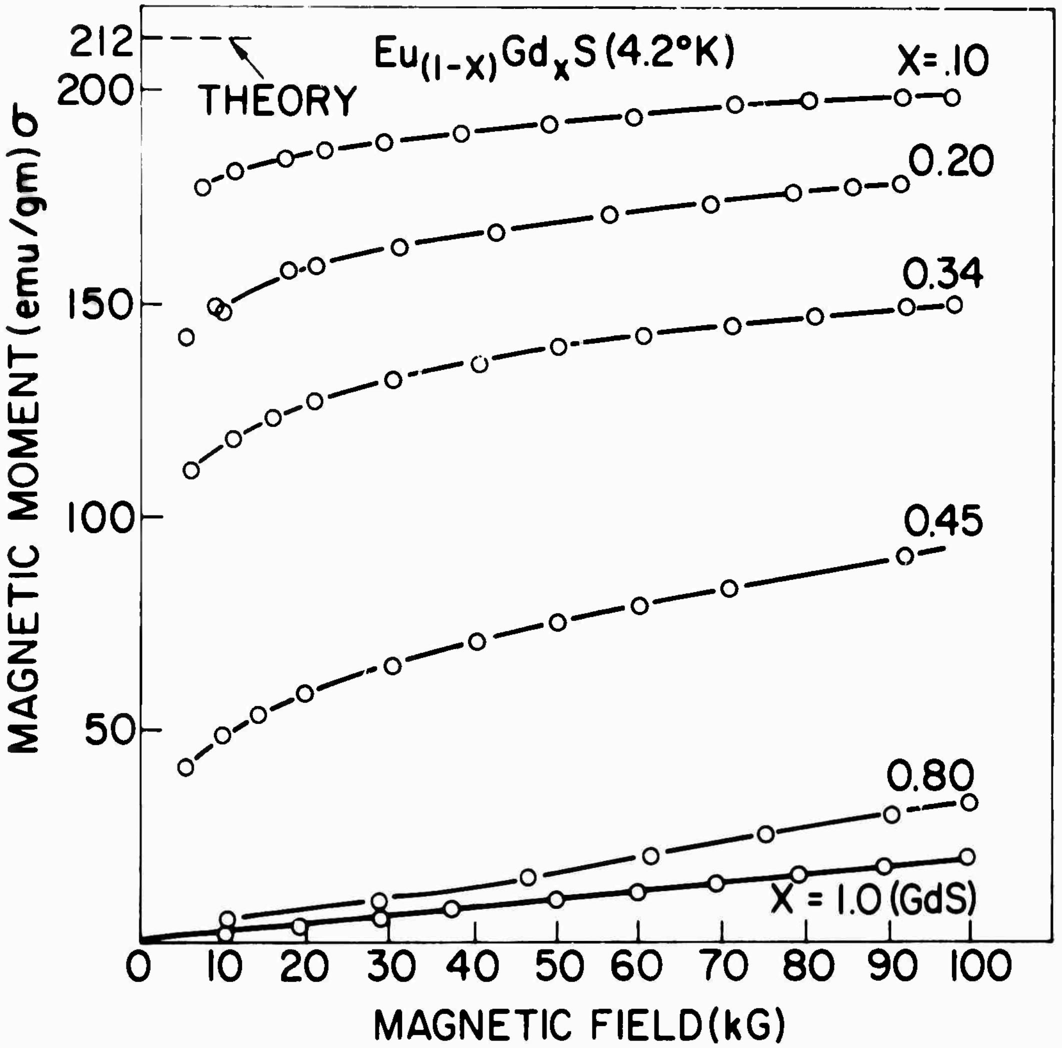

Figure 13. Magnetization curves for selected $Eu_{1-x}Gd_xS$ compositions as a function of a magnetic field.

TABLE VI

Magnetization Data for $Eu_{1-x}Gd_xS$

x	σ $\frac{\text{emu-guass}}{\text{gm}}$	$'_0$ $\frac{\text{emu}}{\text{gm}}$	$'_0$ $\frac{\text{cm}^3}{\text{gm}}$
.085	81.9	186.5	$.143 \times 10^{-3}$
.20	162.3	162.4	.176
.34	173.4	131.6	.217
.45	147.4	59.8	.362
.82			.255
.86	antiferromagnetic		.216
1.00			.200

From the linear decrease of moment (Figure 12) with Gd^{3+} concentration, it is apparent that the gadolinium is not contributing to the total moment. However, in the paramagnetic state, Gd^{3+} is contributing in a normal manner as can be seen from Figure 14. Here the molar Curie constant, C_m, is plotted vs x. Theory gives $C_m = N\mu_{eff}^2/3k$ where N is Avogadro's number, k the Boltzmann constant and $\mu_{eff} = g\beta\sqrt{J(J+1)}$. Eu^{2+} and Gd^{3+} each have $J = 7/2$ and $g = 2$ and a theoretical value of $C_m = 7.85$ is expected. The fact that C_m is somewhat below the theoretical value in the middle compositions possibly means that trivalent europium is present. It is well known that Eu^{3+} has a total quantum number J equal to zero because the spin and orbital contributions cancel each other. (Eu^{3+} has a small field-induced moment, but this is

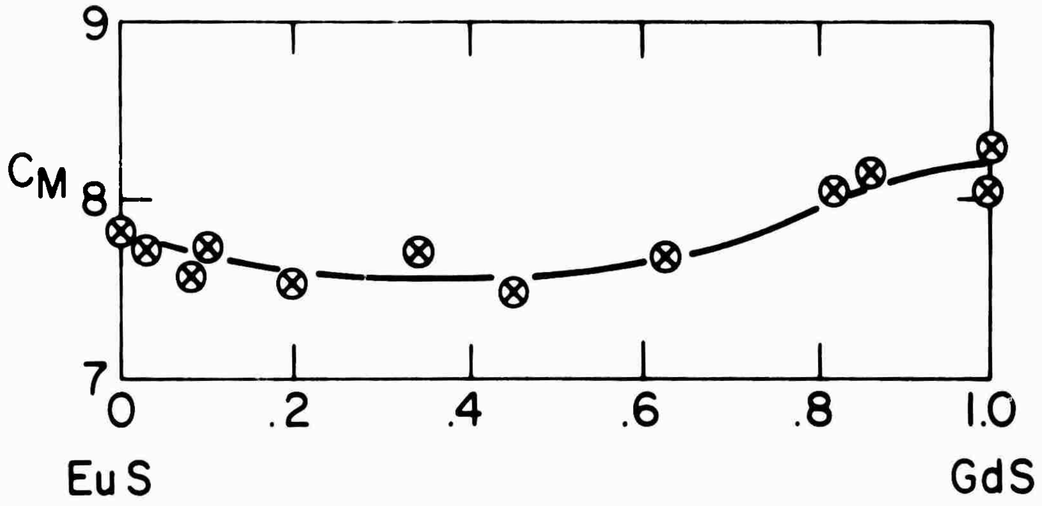

Figure 14: Molar Curie constants of $Eu_{1-x}Gd_xS$ as a function of composition.

negligible compared to the Eu^{2+} moment.) Figure 14 indicates that in the composition range x = 0 to 0.6 an average of 3% Eu^{3+} is suspected. In the region x > 0.8, however, C_m takes on values greater than the theoretical value, showing, on an average, that each ion has a moment about 0.1 μ_B greater than expected. We attribute the additional moment to the polarization of the conduction electrons. This polarization would be induced by the indirect exchange mechanism in which the electrons are involved.

3.1.2 Mangetic Structure

In this section we speculate on a magnetic structure which would fit the data. Two models are illustrated in Figure 15. In discussing the models we will limit the exchange to nearest neighbor interactions, treating the next nearest neighbor exchange as being smaller and less sensitive to both lattice parameter changes and conductivity changes in the system.

Model I is essentially an oversimplification since only two interactions are considered; the Eu-Eu (J_E) and the Gd-Gd (J_G). If we assume J_E is positive and J_G negative, then Model I shows each pair (or cluster) of Gd ions must order antiparallel. Under this condition the measured magnetic moment would be the resultant ferromagnetic Eu contribution. Model I would fit the data (Figure 12) over the range x > 0.3 but in the range x = 0.4 to 0.6, the extra decrease would require special consideration. Model I is essentially a two-phase magnetic structure and the linearity of $1/\chi$ vs. T found in the paramagnetic region (Figure 8) would not be expected.

Model II (Figure 15) is more realistic. It assumes that besides J_E and J_G there is also a Eu-Gd (J_{EG}) interaction which for the moment can be either positive or negative. Either sign leads to a canted type (or spiral[21])

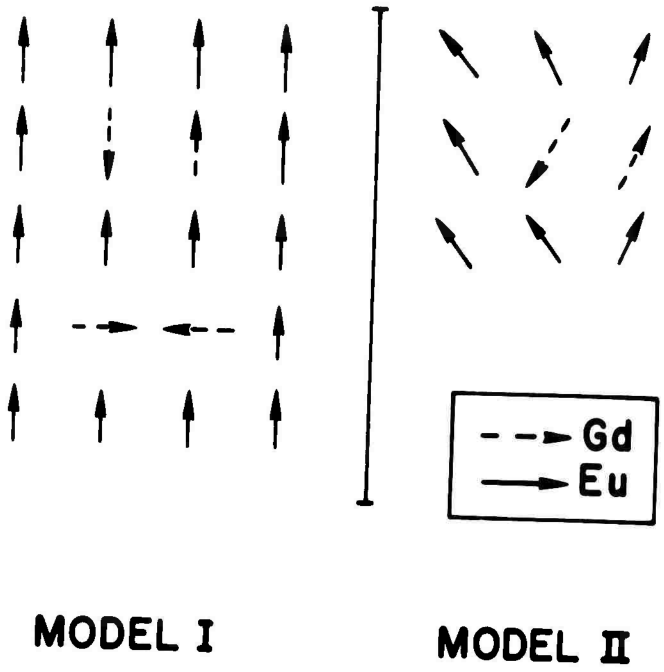

Figure 15: Proposed magnetic structure models for $Eu_{1-x}Gd_xS$.

magnetic structure as shown in the drawing. Taking J_{EG} as positive (and J_E +, J_G -, as before) means that when a Gd ion has a Eu ion neighbor antiparallel there is a rotation of the two ions to minimize the exchange energy. Since each ion in turn is coupled to its own neighbors, we end up with a structure whose magnetic moment is lowered by the amount of canting. The exchange energy between two atoms with total spins S_1 and S_2 has the form $J \underset{\sim}{S}_1 \cdot \underset{\sim}{S}_2$ and depends on the cosine of the angle between the spins. Thus for a spin assembly with several exchange interactions, the average angle between spins to minimize the exchange energy will vary as some value of sine or cosine with composition. The decrease in moment with Gd^{3+} concentration would, therefore, not be linear in x but vary in some more complex way.

If we now examine the values for the linear term $\chi_0 H$ (see Table VI) we see that a maximum occurs around the cross-over point where [illegible] goes from plus to minus, a condition where the exchange forces balance out. It is under these conditions that the applied field is most effective in rotating the canted system ion moments against the exchange interactions. Model II qualitatively fits the magnetic properties but a more quantitative interpretation is necessary for final evaluation.

3.2 Photoconductivity Mechanisms in the Magnetic Semiconductor EuSe

Thermally activated photoconduction has been observed in the paramagnetic phase of EuSe (T_N = 4.6°K) by both steady state and transient measurements. The transient measurements show that it is the photomobility and not the relaxation which is activated. The photoconductive decay tends to be long, nonexponential, sample dependent, and independent of temperature and magnetic field, below 100°K. The activation energy (several hundredths of an eV) is at least partially magnetic in origin, for it can be decreased significantly by a magnetic field. Of particular interest is the similarity of the results to the dark conductivity of 1% Gd doped EuSe in the paramagnetic phase.[22] This connection has been previously noted with respect to the steady state photoconduction.[23]

It appears that photoelectrons in undoped EuSe conduct in much the same manner as do impurity electrons in doped EuSe. In doped material, activated conduction in the paramagnetic region has been explained in terms of hopping between impurity sites.[24,25] An electron, bound near an impurity, causes nearest and next nearest neighbor Eu spins to be partially aligned due to the strong s-f exchange interaction, lowering the electron exchange energy. An electron bound to an impurity by the coulomb interaction thus has an additional binding energy, magnetic in origin. The result is a magnetic impurity state (MIS). In the model, it is the magnetic binding energy which is the activation energy for hopping, but it is the Coulomb energy which causes the localization to begin with.

Since our undoped material has impurities in concentration 10^{-3} - 10^{-4}, it is natural to construct a similar defect model for photoconductivity. In this model, electrons are excited from localized f levels in the band gap to f-hole d-electron exciton states degenerate with the s-band.[24,26] The exciton breaks up and the electron rapidly relaxes to the bottom of the conduction band and then to an excited state of a deep defect or to a shallow defect.

Activated conduction then occurs by hopping in the shallow states or by thermal excitation to the band. Conduction ends when the electron relaxes to a deep defect state which acts as a recombination center. Spin clusters form around the occupied defect states, that is they are MIS similar to those proposed for doped material. The activated conduction will be magnetically sensitive just as in the case with doped material.

In this model the long, temperature and magnetic field independent, photodecay results from the decay of an electron in a shallow level associated with one defect to a deep level associated with another defect. Since there will be a distribution in space between defects there will be a distribution in decay times. Since the relaxation is between defects, it will be slow.

For steady state photoconductivity we may write,

$$(I_{dc}/V)\ (\ell/w)\ (E/P) = \sum_i \beta_i \mu_i \tau_i, \tag{12}$$

where I_{dc} and V are the steady state current and voltage. ℓ and w are the sample length and width. E is the photon energy and P the power per unit area of radiation absorbed by the sample. β_i, μ_i and τ_i are the quantum efficiency, mobility and lifetime for a component, i, of the photocurrent. A similar expression,

$$(I_T/V)\ (\ell/w)\ (E/W) = \sum_i \beta_i \mu_i, \tag{13}$$

may be written for the transient case, where a pulse of light short with respect to the lifetime τ_i is used. I_T is the current immediately following the pulse and W is the energy per unit area at the sample.

Transient photoconductivity measurements have been made using a xenon flash which has 0.8 of its energy in 10^{-5} sec or a dye laser with a 2 x 10^{-6} sec pulse.

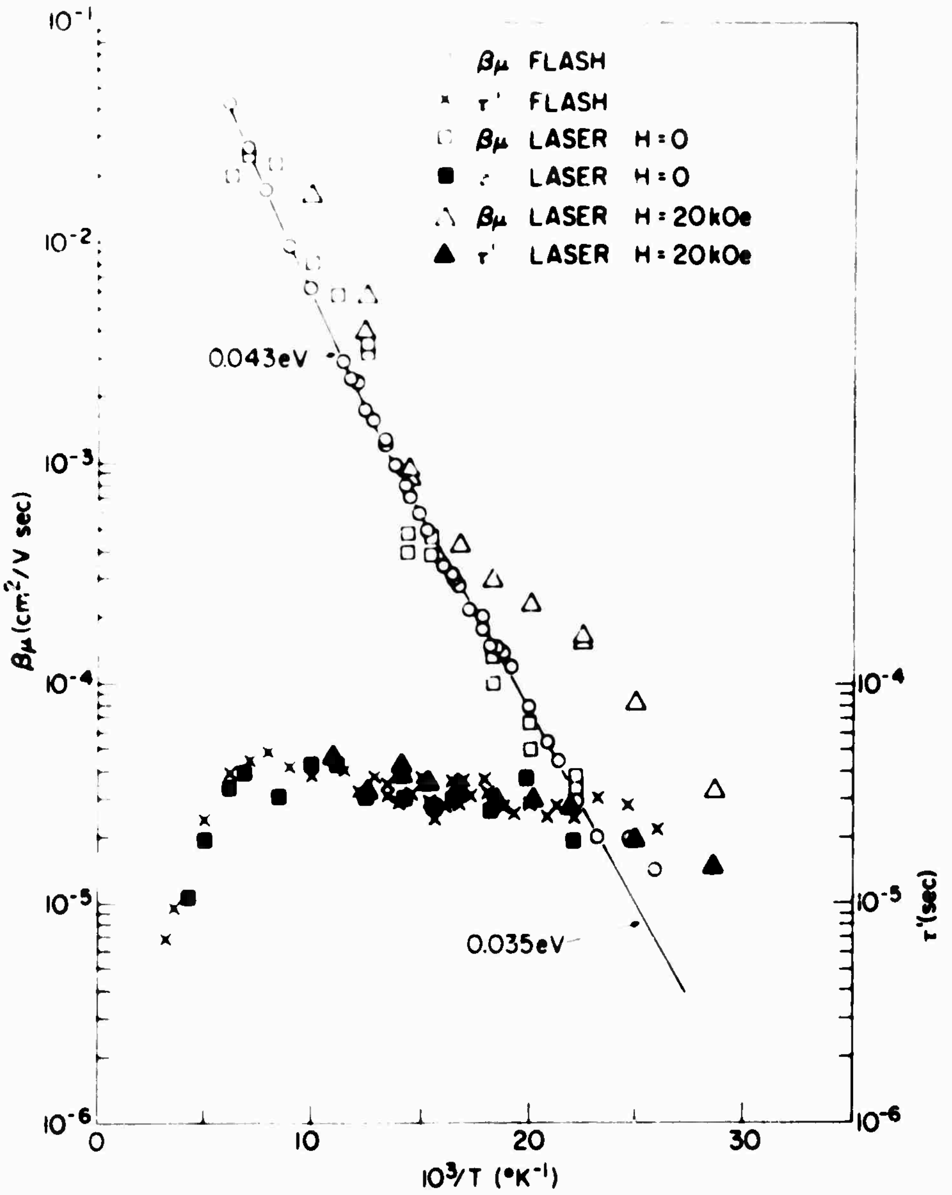

Figure 16 $\beta\mu$ and τ' vs inverse temperature for EuSe. White light source is a Xenon flash at 10^{-4} J/cm^2. Dye laser source is 2.12 eV at 3×10^{-5} J/cm^2. Bias is 100V. $\beta\mu$ = 0.1 corresponds to 10^{-3} amp for the laser with 100V bias. Current and decay are measured at 10^{-5} sec. The slopes are indicated in eV.

The current amplitude at 10^{-5} sec is taken as a measure of $\beta\mu$, and the time, τ', to fall to 1/e of that value is its initial decay after the pulse. The results are shown in Figure 16 for both white flash and dye laser excitation.

The data of Figure 16 show a number of interesting results. The $\beta\mu$ product is thermally activated, while the response time, τ' is constant below 80°K. The activation energy is similar to that of the d.c. photocurrent measurements and the dark conductivity of Gd doped EuSe in the same temperature range.[22,23] Also, the $\beta\mu$ product increases with an external magnetic field, H, while τ' does not. The model described earlier is in agreement with these results since it predicts a thermally activated mobility and temperature independent response time, τ' equal to the lifetime, τ.

From these results we conclude that the final state of the optical absorption (f-d exciton) lies degenerate with, or above, the shallow defect states responsible for photoconduction. A shallow defect state will trap an electron which then causes a spin cluster to form around it. The result is an additional magnetic binding energy exactly like that proposed for Gd doped EuSe. Conduction then occurs either by hopping within the shallow defect states or by thermal excitation to the band. Conduction ends when the electron relaxes to a deep defect state.

The conditions for the above model are as follows. In Gd doped EuSe, the deep defects (Gd) must be sufficiently numerous ($\sim 10^{-2}$) so that their wave functions overlap enough for hopping but not so much that impurity banding takes place. There must be some compensation so that there are empty sites to hop to. In undoped EuSe, the deep defects must be sufficiently scarce (10^{-3} - 10^{-4}) so that hopping is unimportant. However, shallow defects with larger wave functions should be present in an amount (10^{-3} - 10^{-4}) so that impurity banding is not possible and hopping may or may not be possible. In the latter case, the electrons conduct by excitation to the band. Some compensation is required so that holes in deep states will be available for recombination and their number will be independent of the light intensity.[27]

3.3 The Insulator-Metal Transition and Long Range Magnetic Order in EuO

In europium-rich EuO, the conductivity may increase by many orders of magnitude as the temperature is decreased below the ferromagnetic ordering temperature (T_c = 69.3°K). This behavior has been reported by Oliver, et al[28,29,30] and by Petrich, von Molnar and Penney[31]. We have extended the measurements to cover a wider range of conductivities both with and without an applied magnetic field. The results are shown in Fig. 17. It is evident that this insulator metal transition just below T_c is related to the onset of magnetic order. It is our purpose to explore the nature of this relationship.

The crystal (89B) used to obtain the data of Fig. 17 was grown in the following way. Eu_2O_3 pellets were placed in an open tungsten crucible which was in turn placed in a larger sealed tungsten crucible with a 100% excess of Eu metal over that required to make stoichiometric EuO by the reaction Eu_2O_3 + Eu. Liquid phase metal was not in contact with the Eu_2O_3 pellets or the crystals which were subsequently formed. The reaction was, therefore, only through the Eu vapor. This double crucible arrangement was heated to 1650°C, held for 16 hours, cooled slowly to 1350°C and then rapidly to room temperature. EuO crystals and some excess Eu metal were found in this inner crucible.

Another technique was used to grow the crystals (73) used in Ref. 31 which showed conductivity behavior similar to Fig. 17. Eu_2O_3 was reacted with a large excess of Eu metal at 1100°C in an open W crucible. The result was EuO and Eu vapor which distilled off. This EuO was sealed in a closed W crucible with Eu metal and heated to 2070°C. It was cooled slowly (16 hrs.) to 1200°C and then rapidly to room temperature.

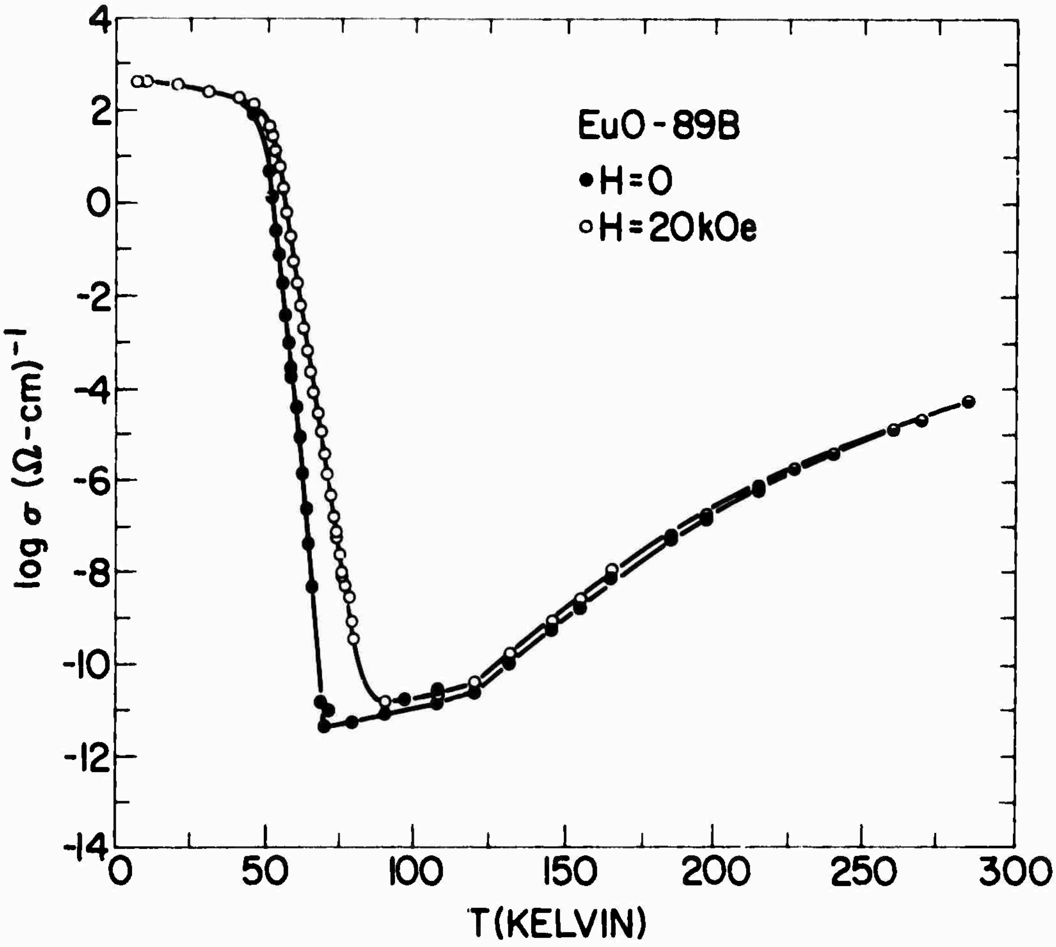

Figure 17: Conductivity vs. temperature for EuO sample 89B in 0 and 20 kOe.

A third technique was used to grow crystals 89A which also showed behavior like Fig. 17. Eu_2O_3 + 2Eu was sealed in a W crucible and heated to 2000°C. It was cooled to 1700°C in 16 hrs. and then rapidly to room temperature. Since all three methods use excess Eu, it is likely that the resulting crystals contain oxygen vacancies. More detail on this point is included in Section 2.1 of this report.

For conductivity measurements, LaAg contacts were alloyed into the material under an inert He atmosphere and provided good ohmic contacts. Wire leads were attached to these contacts with In solder. The conductivity measurements were all made using the four probe van der Pauw technique.[32] Two Keithly electrometers were used to monitor the current and voltage. A guarded circuit was used so that current leakage through connectors and feedthroughs was not measured. Current leakage on the surface of the sample and sample holder limited our measurements to about $10^{13}\Omega$ corresponding to bulk conductivities of about $10^{-11}(\Omega\text{-cm})^{-1}$.

A cleaved surface of the sample was attached to a copper sample holder using a thin layer of Apiezon N grease. The temperature of the sample holder was measured using a Pt resistance thermometer above 15°K and an Allen Bradley 1/8 watt 1100Ω resistor below 20°K. An Air Products and Chemicals liquid transfer refrigerator was used to achieve temperatures from 4K to 300K. A GaAs diode thermometer and P.A.R. controller were used for temperature control.

The conductivity, σ, shown in Fig. 17 may be divided into four regions. Above 130°K, log σ, if plotted against 1/T, shows thermally activated conduction with a 0.285 eV activation energy. Between 70°K and 125°K the conduction is very small and of undetermined origin. Below T_c, there is a thirteen order of magnitude increase in σ which we may well call an insulator metal transition. Below 40°K conduction is essentially metallic.

Hall effect measurements have been made at 5°K and room temperature but not in the 40 to 70°K region due to the large magnetoconductance. The results give a carrier concentration, n, of $10^{19}/cm^2$ at low temperature and 10^{14} at room temperature. It appears, therefore, that the sharp increase in conductivity, $\sigma = ne\mu$, below 70°K is due to a change in n and not mobility, μ. The Hall effect and conductivity data for these samples showing the insulator metal transition are summarized in Table VII. The expression $\sigma(T) = \sigma_\infty \exp(-E/kT)$ defines σ_∞ and E in terms of the data, $\sigma(T)$. Hall measurements on sample 73 between 225 and 295°K show that it is n that is changing exponentially.

Oliver[29,30] has compared the infrared free carrier absorption, $\alpha \sim n\lambda^2/m^*\tau$, to the conductivity $\sigma = ne^2\tau/m^*$ and has determined that the large change in σ below 70°K is due to a change in n and not $\mu = e^2\tau/m^*$ assuming m^* is constant. Our Hall data supports this conclusion. In EuO the optical absorption edge shifts several tenths of an eV to lower energy. This red shift begins well above T_c and follows the short range magnetic order, $\langle S_i \cdot S_j \rangle$[33,34]. According to the model of Oliver, Kafalas, Dimmock and Reed[28,29,30], the optical absorption edge corresponds to a transition from an atomic f level lying in the band gap to the conduction band and, therefore, the red shift indicates that the conduction band decreases in energy, relative to tightly bound atomic like levels, following the short range order. They postulate that there are trap states associated with oxygen vacancies, $\boxed{O}$. The energy of an electron in such a trap will be independent of magnetic order if it is very well localized and has no overlap with neighboring Eu spins. They propose, then, that the activation energy, E, to promote electrons from the traps to the conduction band decreases by several tenths of an eV following the red shift and the short range order. The decrease in E causes an exponential increase in n and σ according to

$$n(T)/n(0) = \sigma(T)/\sigma(0) = \exp(-E/kT) \qquad (14)$$

in the region of the insulator-metal transition.

We have tested this model and find that the data are consistent with Eq. 14 but E decreases with the magnetization, M, that is the long range order, $\langle S \rangle$, rather than the short range order $\langle S \cdot S \rangle$.

The data of Fig. 17, $\sigma(T)$ at $H = 0$, may be used with Eq. 14 to determine experimental values for $E(T)$. In order to test the relationship between E and $\langle S \rangle$ we need $\langle S(T) \rangle$. The hyperfine field $h(T)$ is proportional to $\langle S(T) \rangle$ and has been measured by Petrich[31] on EuO-73. It is given by

$$\langle S(T) \rangle / S(0) = h(T)/h(0) = 1.13 \times (1-T/69.3)^{0.36} \qquad (15)$$

in the range 40-70°K. Sample 89B also has a Curie temperature of 69.3°K determined by zero field extrapolation of M^2 vs. H/M plots of magnetization data taken at 4 to 10 kOe in the neighborhood of T_c. The exponent $\beta = 0.36$ is the same as that given by Menyuk, Dwight and Reed[35] as determined from magnetization measurements on EuO. We will assume, therefore, that Eq. 15 is valid for 89B as well as 73. The data of Fig. 17 used with Eqs. 14 and 15 determine the dependence of the activation energy for conduction on the long range order $\langle S \rangle$. The results, as shown in Fig. 18 are:

1) $E(T)$ vs. $\langle S \rangle$ is a straight line;

2) the intercept at $\langle S \rangle = 0$ is 0.30 eV;

3) $\langle S \rangle / S(0) = 0.77$ where $E \to 0$.

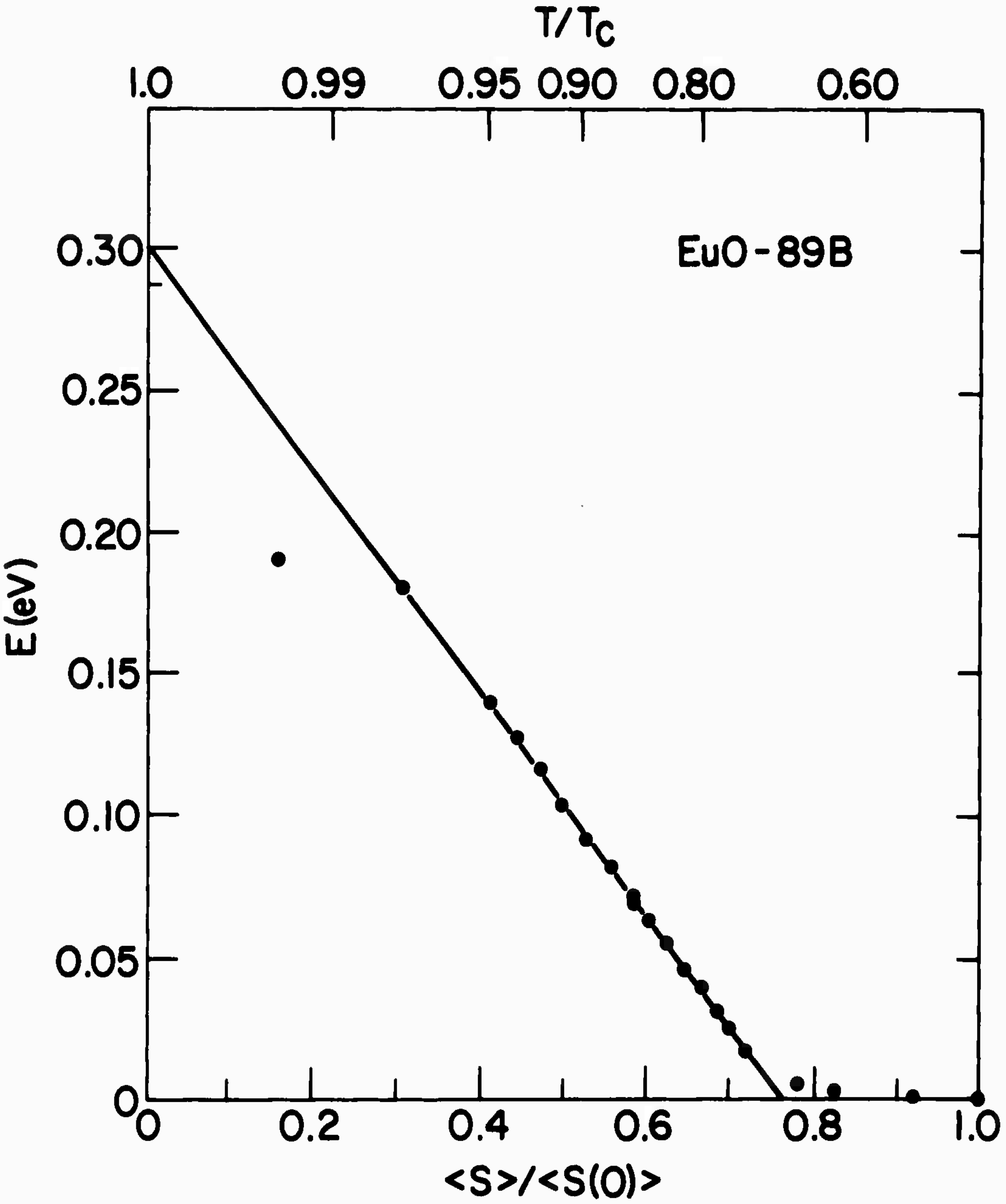

Figure 18: Activation energy vs. magnetic long range order for EuO sample 89B.

The first result shows that the activation energy E is linearly dependent on long range order $\langle S \rangle$. A similar plot of E vs. short range order $\langle S \cdot S \rangle$ is not a straight line. The enormous increase in n and σ below T_c is, therefore, caused by a decrease in E which is linearly proportional to the increase in $\langle S \rangle$. The second result indicates that the Fermi level, E_f, lies about 0.30 eV below the band edge for all temperatures where $\langle S \rangle = 0$, that is $T \geq T_c$. In fact the $\sigma(T)$ data above 130°K obeys an exponential of the form Eq. 14 with E = 0.285 eV in remarkable agreement with the 0.30 eV value extrapolated from the low temperature data. The third result gives a measure of the exchange coupling, J, between band electrons and the europium 4f spins, S, as we shall see. The point where $E \to 0$ corresponds to the knee at about 40°K in Fig. 17. Below this temperature since E = 0 the conduction is not thermally activated but rather metallic, as observed. These results may be summarized by the expression

$$E = E_0 - A\langle S \rangle = 0.30 - 0.39 \langle S \rangle / S(0) \text{ eV}. \qquad (16)$$

The magnetoconductance in the neighborhood of T_c is very large. The ratio $\sigma(0)/\sigma(H = 20 \text{ kOe})$ at T_c as shown in Fig. 17 is about 10^6. It is interesting to consider whether Eq. 16 is applicable in an external field. The 20 kOe data of Fig. 17 may be used to determine an activation energy using Eq. 14 which in turn may be used to predict $\langle S(T, 20 \text{ kOe}) \rangle$ by Eq. 16. The 20 kOe results are plotted as open circles in Fig. 19 along with the zero field data obtained the same way. The fit of the zero field data (points) to the solid line ($\langle S \rangle / S(0)$ or $M/M(0)$) through the points is equivalent to the fit in Fig. 18.

The magnetization of a sphere made from the same crystal run as

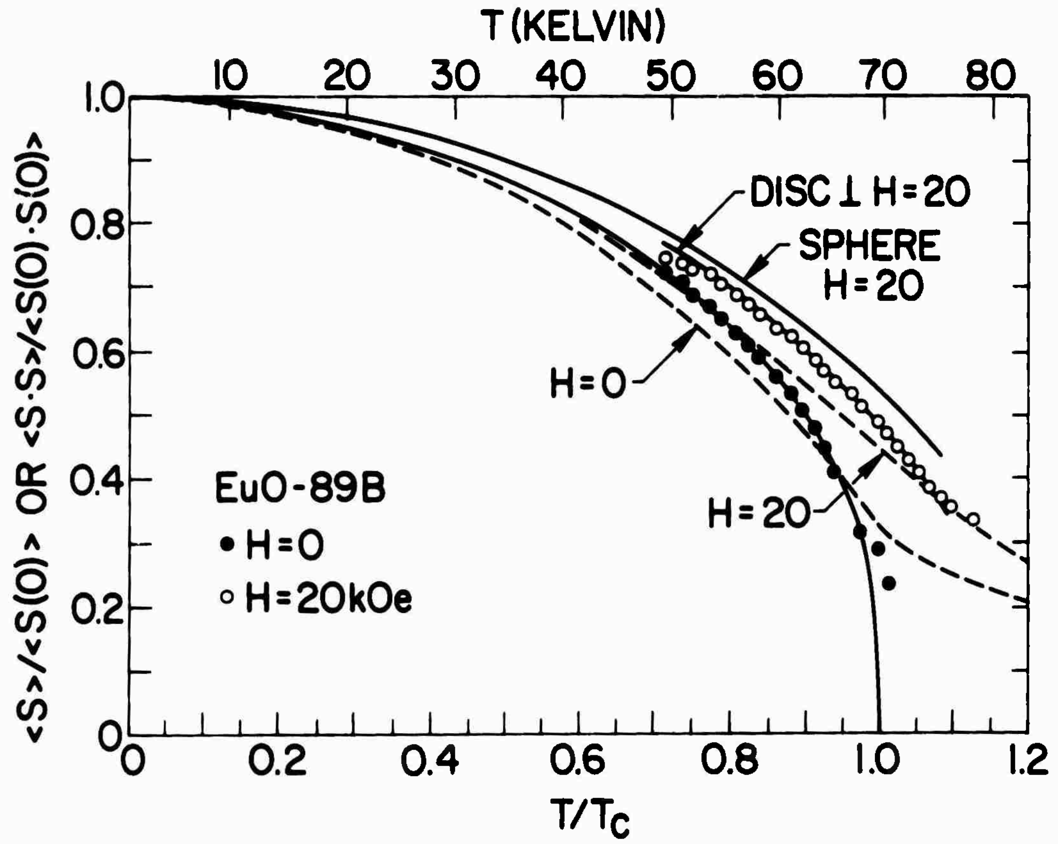

Figure 19: Magnetization or long range order (solid lines) vs. T measured for a sphere in H = 0 and H = 20kOe as well as long range order calculated for a disc perpendicular to 20kOe. Also shown is measured isotropic short range order (dashed lines) in H = 0 and H = 20kOe. The predicted values of <S> from conductivity data are shown for H = 0 (dots) and H = 20kOe (circles).

that used for the conductivity measurements has been measured as a function of temperature and field. The data for an applied field, H^a, of 20 kOe is shown in Fig. 19 and labelled "sphere H = 20". The internal field is $H^i = H^a - 4\pi M/3$. From this data we may calculate what the magnetization would be for a disc magnetized perpendicular to a 20 kOe field using $H^i = H^a - 4\pi M$. The data points for $\langle S(T, 20\ \text{kOe})\rangle$ (open circles) as determined from σ (20 kOe) are in good agreement with the solid line for a disc $\perp$ H = 20 kOe inferred from the magnetization measurements. The actual sample used is a rectangular solid 0.030 x 0.034 x 0.010 inches with the field parallel to the 0.034" edge. The four van der Pauw contacts were on one of the largest faces. Since the sample is not an ellipsoid it will not have uniform magnetization. Over the sample, $M(r)$ may vary between a maximum which is that applicable for a disc $\parallel$ ($H^i = H^a$) and a minimum which is that applicable for a disc $\perp$ ($H^i = H^a - 4\pi M$). Equations 14 and 16 show that variations in M will cause exponential variations in σ. The average σ which is measured along a constant current path will correspond to an average of $\sigma^{-1} = \rho = \rho_0 \exp(E_0 - A\langle S\rangle)$ according to Eqs. 14 and 16. This highly non-linear average can be approximated by using the maximum $E = E_0 - A\langle S\rangle$ that is the minimum magnetization rather than an average magnetization. The magnetization predicted by the σ (T,20 kOe) data is, therefore, close to the minimum possible value, that is, a disc perpendicular to H^a as shown on Fig. 19.

Also shown on Fig. 19 is the short range order, $\langle S \cdot S\rangle$, for H = 0 and 20 kOe as measured by Argyle, Miyata and Schultz[36,37]. It is apparent that the conductivity data follows the long range order rather than the short range order.

The conductivities at H = 0 for $70 < T < 125$°K and at H = 20 kOe for $80 < T < 125$°K do not fit Eqs. 14 and 16 as does the rest of the data. These very

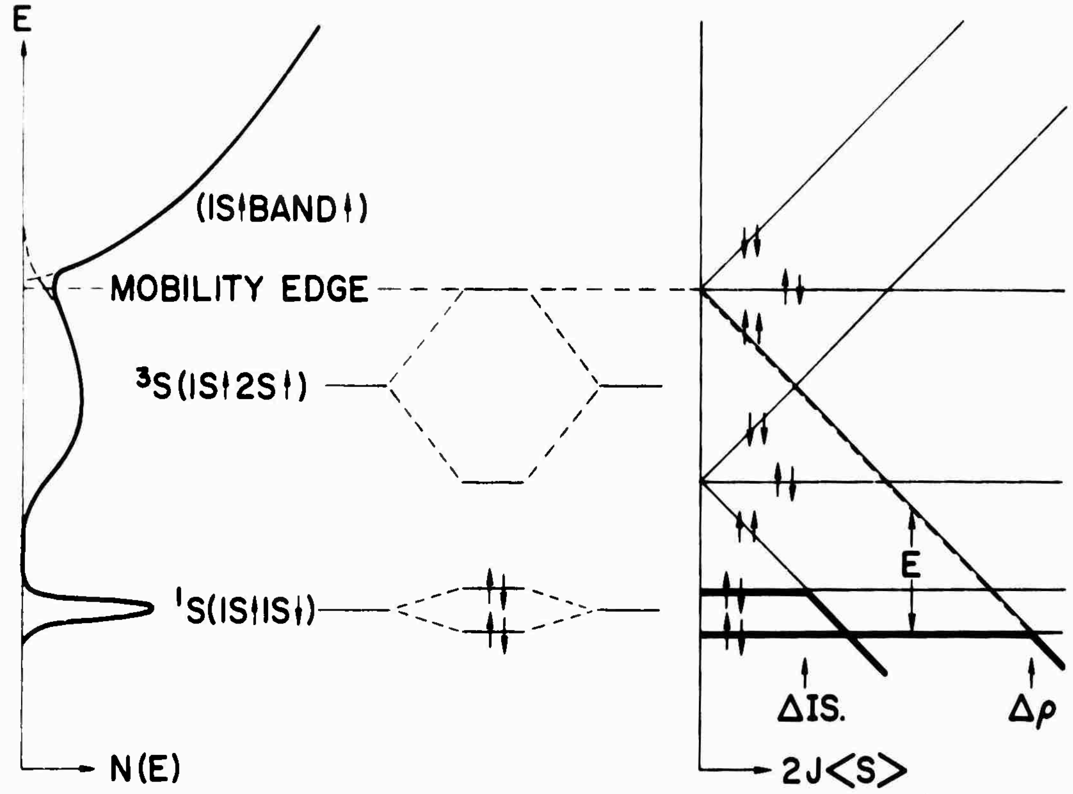

Figure 20: The center diagram shows the states resulting from two interacting vacancies, [0]. The left diagram shows the two electron density of states which results from a random distribution of vacancies. It is assumed that one electron is always in a 1s state and the second may be 1s, 2s or in the band. The right diagram shows the dependence of these states on magnetic order, <S>.

low values correspond to some other weak conduction process or to current leakage on the sample surface or sample holder.

Kasuya[38] has proposed a model somewhat different from that of Oliver et al.[28,29,30] The trap state associated with the $\boxed{O}$ may contain two electrons since $\boxed{O}$ differs by two charges from $O^{=}$. The trap may be thought of as a helium-like defect rather than the common hydrogenic defect suitable for Gd^{3+} substituted for Eu^{2+} or Cl^{-} substituted for $O^{=}$. The lowest helium-like state is a non-magnetic singlet ^{1}S with configuration 1s↑, 1s↓. The first excited states are magnetically active triplets, ^{3}S(1s, 2s). A large magnetic field such as the exchange field, if sufficiently large, will split the ^{3}S so that the lowest branch ^{3}S(1s↑, 2s↑) lies below the ^{1}S (1s↑, 1s↓) and the electronic configuration will change. If some of the ^{3}S states are merged with the bottom of the conduction band, conduction will result. In Ref. 31 it was shown that the electronic configuration (isomer shift) began to change at low <S> (0.99 T_c) but that the knee of the σ (T) curve did not occur until higher <S> (0.7 T_c). These results may be interpreted within Kasuya's model in the following way. Since there is a distribution in the defect-defect distance, there will be a distribution in the energies of the ^{3}S states as shown to the left in Fig. 20. The two interacting defect states are shown schematically in the center of Fig. 20. For a sufficiently high density of defects, some of the ^{3}S states will be hybridized with the band and will be conducting while others will lie below the mobility edge and be non-conducting but still be more extensive than the ^{1}S states. As shown on the right in Fig. 20, the long range order <S> will gradually drive the ^{3}S (1s↑2s↑) states below the ^{1}S producing initially an isomer shift, ΔIS, and finally the insulator-metal transition, $\Delta\sigma$. Quantitatively, if the exchange interaction is

$$H = -2J\vec{s}\cdot\langle\vec{S}\rangle \quad , \qquad (17)$$

then the energy difference ΔE between the ^1S (trap) states and the ^3S conducting states is

$$\Delta E = \Delta E_0 - 2J\langle S\rangle \qquad (18)$$

which is exactly the form we have derived experimentally. The long range order $\langle S\rangle$ enters because the conducting electrons are in a band and are, therefore, spread out over a long range. The Fermi level may be pinned at the ^1S levels or it may lie halfway between the ^1S and ^3S states, therefore, our measured $E = \Delta E$ or $E = 1/2\ \Delta E$.

With this model we may return to the third result that $\langle S\rangle/S(0) = 0.77$ at $E = 0$ and using $S(0) = 7/2$ and $E_0 = 0.30$ find $J = 0.055$ eV or $J = 0.11$ eV corresponding to $E = \Delta E$ or $1/2\ \Delta E$. Von Molnar and Shafer[39] have measured the spin disorder scattering in metallic EuO doped with Gd and find $J \approx 0.05$ eV assuming $m^* = 1$. This agreement for two different types of measurement is encouraging.

In reference 31, both Mössbauer and conductivity measurements were reported for samples made from the same crystal run (#73). Therefore, T_c, $\langle S(T)\rangle$, and $\sigma(T)$ were all known for similar crystals. An analysis like that described above gave a plot similar to Fig. 18 with the following results:

1) E vs. $\langle S\rangle$ is a straight line;
2) the intercept at $\langle S\rangle = 0$ is 0.29 eV;
3) $\langle S\rangle/S(0) = 0.72$ where $E \to 0$.

These results are similar to those for sample 89B. The room temperature activation energy for 73 is 0.30 eV in good agreement with the low temperature extrapolation of 0.29 eV. The third result gives J = 0.057 or 0.115 depending on whether E = ΔE or 1/2 ΔE as before.

Although the data presented here and in Ref. 31 does not prove that Kasuya's model is correct, it is consistent with that model. What we have shown is that the insulator metal transition may be understood in terms of thermally activated carriers (Eq. 14) and an activation energy linearly dependent on long range magnetic order (Eq. 16) both with and without an external magnetic field. The data is not consistent with an interpretation based on short range order.

The low temperature data, when plotted as activation energy vs. long range order (Fig. 18), may be used to predict a high temperature value for the activation energy of 0.30 eV in good agreement with the measured high temperature value of 0.285 eV. The low temperature conductivity data may also be used to determine the exchange coupling, J, between a conduction electron and the Eu 4f spins. J is .05 or .011 eV, depending on the model. These values are in order of magnitude agreement with a previous determination made from resistivity measurements in degenerate EuO.

TABLE VII

Hall and Conductivity Data

Sample	89B	73	89A
$\sigma(287°K)$ $(\Omega\ cm)^{-1}$	5.3×10^{-5}	1×10^{-4}	6.17×10^{-5}
$\mu(287°K)$ $cm^2/v\text{-}sec$	9	14	11
$n(287°K)$ cm^{-3}	4×10^{14}	4.5×10^{14}	3.5×10^{14}
E(287°K) eV	0.285	0.30	0.30
σ_∞ $(\Omega\text{-}cm)^{-1}$	3.5	21	12
$\sigma(5°K)$ $(\Omega\text{-}cm)^{-1}$	430	500	770
$\mu(5°K)$ $cm^2/v\text{-}sec$	70	130	170
$n(5°K)$ cm^{-3}	4×10^{19}	2×10^{19}	3×10^{19}

3.4 Transport Properties of Metallic Rare Earth Chalcogenides

It has been found convenient to separate the europium chalcogenides into two major categories, depending on dopant concentration. For $Eu_{1-x}D_x$ Ch, where Ch is the chalcogenide and D is the dopant, if x 0.01 the material in general has semiconducting properties, whereas if x .01 metallic behavior is generally observed. We have, during the past year, carried out experiments in both regions.

In the semiconducting region, the problems associated with measuring and interpreting transport properties are severe, first because either chalcogen or rare earth defects, or both, as well as trivalent rare earth dopants, contribute to conduction and because in many cases only the resistivity is measurable.

Since a knowledge of the specific composition is necessary to relate carrier number to transport and magnetic properties, a series of homogeneous ceramic samples of $Eu_{1-x}Gd_xS$ containing accurately known amounts of trivalent rare earths were prepared under varying Eu pressures. Thermoelectric power and resistivity were studied near and above room temperature. It was concluded that the samples measured fell into two general classes. The majority were p-type with activation energies varying from 0.26 to 0.49 eV and resistivities greater than 10^5 Ω-cm. The remaining samples were highly conducting and n-type, representing materials with large Gd concentrations and/or anneals under high Eu pressure. Although no specific relationship between transport and method of preparation has evolved, the results suggest conditions for the observation of n-type conductivity in EuS.

In the metallic region, our purpose was to try to understand and measure the exchange interaction between free electrons and the localized spin of the rare earth ion. The experiment consisted of measuring the resistivity, Hall effect, and thermoelectric power of EuS:Gd, GdS, LaS and YS single crystals as a function of temperature. The Hall effect and thermoelectric power yield the free carrier number and a rough measure of the Fermi energy E_F on the assumption that a simple parabolic band description is valid, and that the dominant scattering mechanism is known. An estimate of the effective mass can then be made. The temperature dependence of the resistivity can be analyzed to obtain a value for the exchange interaction I_{c-f} between the conduction electrons and the localized ionic spin.[41] This is accomplished with the use of the relation[42]

$$\rho_\infty = 2.7 \times 10^{-4} u \left(\frac{10^{23}}{N}\right) S(S + 1) \frac{I^2_{c-f}}{E_F}, \qquad (19)$$

where ρ_∞ is the magnetic contribution at high temperatures, N is the number of magnetic ions/cc, u the effective mass ratio, and S the spin of the magnetic ion. Because the thermoelectric power of the metals GdS and LaS was small and its variation with temperature complicated, so that no measure of u was possible, the analysis was made, therefore, by assuming a value of u = 1. We expected to obtain large differences between I_{c-f} in EuS:Gd and GdS and no magnetic effect in LaS, since the latter contains no localized spins other than accidental impurities. The former two materials differ in that present evidence indicates that the free carriers are s-like in doped EuS and d-like in GdS.[43] These expectations were in part borne out by experiment, although the values for I_{c-f} quoted below must be regarded as rough estimates. The results of our efforts and our conclusions concerning

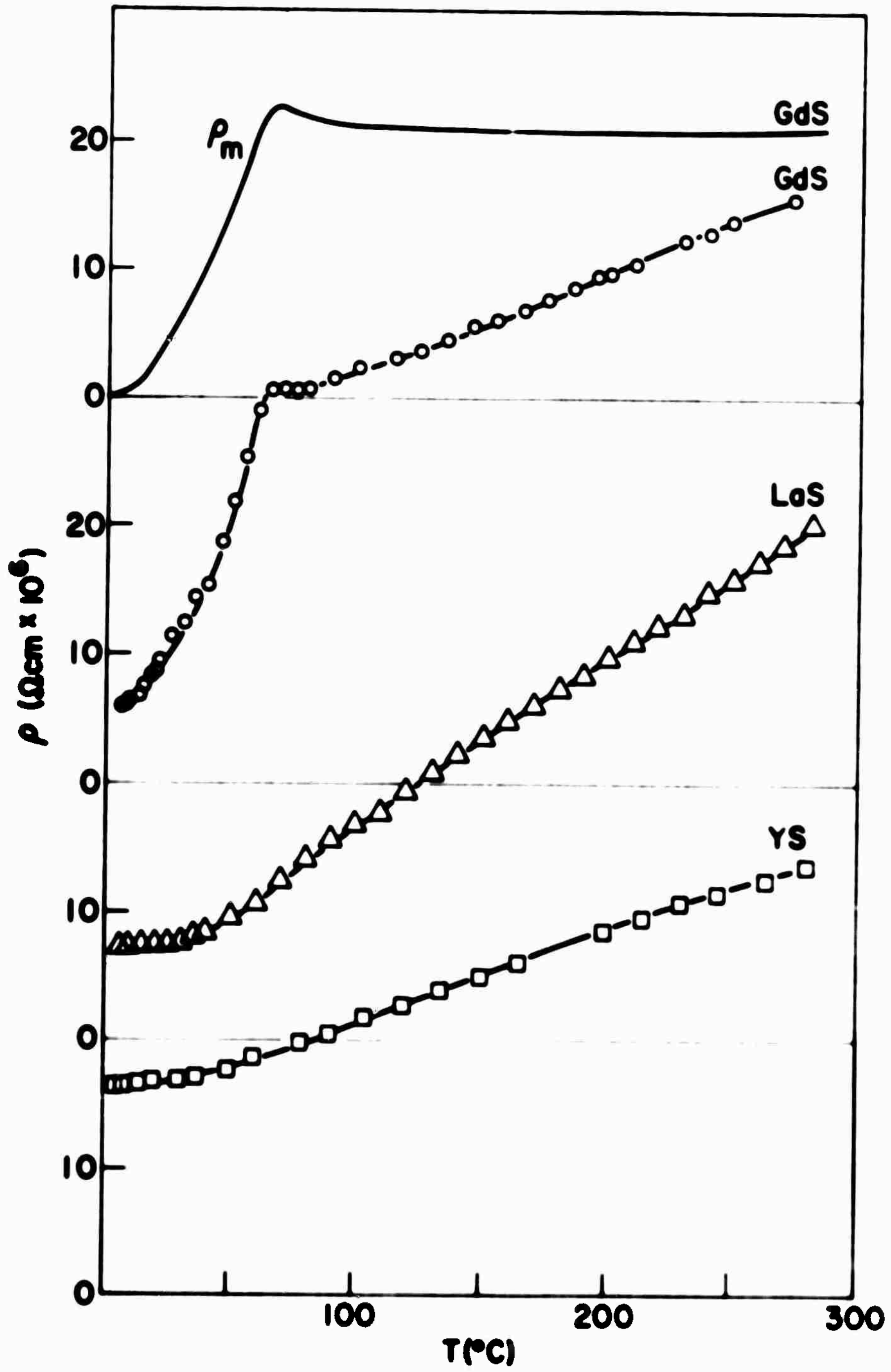

Figure 21: Resistivity ρ of GdS, LaS and YS and the magnetic part ρ_m of the resistivity of GdS as a function of temperature.

these degenerately doped or metallic samples are discussed in the following paragraphs.

3.4.1 Results

Fig. 21 displays the temperature dependence of the resistivity for the three metals, GdS, LaS and YS. Included also is the magnetic part of the resistivity, ρ_m, of GdS which remains after impurity and lattice contributions, ρ_i and ρ_L respectively, have been subtracted. The major features of the curves are: i) LaS and YS, which are non-magnetic but of the same structure and electronic configuration as GdS, exhibit a temperature dependence which follows the classic Bloch-Grüneisen form.[44] ii) The magnetic part of the resistivity exhibits a small increase near the Neel temperature (T_N = 50°K) of this antiferromagnet. iii) Impurity scattering ($\rho_i = \lim_{T\to 0^\circ}$) is comparable and $\sim 10^{-5}\,\Omega$-cm in all samples.

From i) we can infer the Debye temperatures, θ_D, of 210°K for both LaS and YS. θ_D for the isomorphic compound EuS derived from the lattice specific heat[45] is 208°K. Taking into account the differences in cubic axes and in mass of the metal-ions for the different compounds, we obtain surprising agreement between these values, particularly since θ_D deduced from the two measurements tend, in general, to differ somewhat.[46] Furthermore, i) demonstrates the validity of writing the expression

$$\rho(T) = \rho_i + \rho_L(T) + \rho_m(T), \tag{20}$$

which is necessary to deduce ρ_m. Here it is assumed that ρ_i is independent of T and ρ_L follows a Grüneisen curvature.

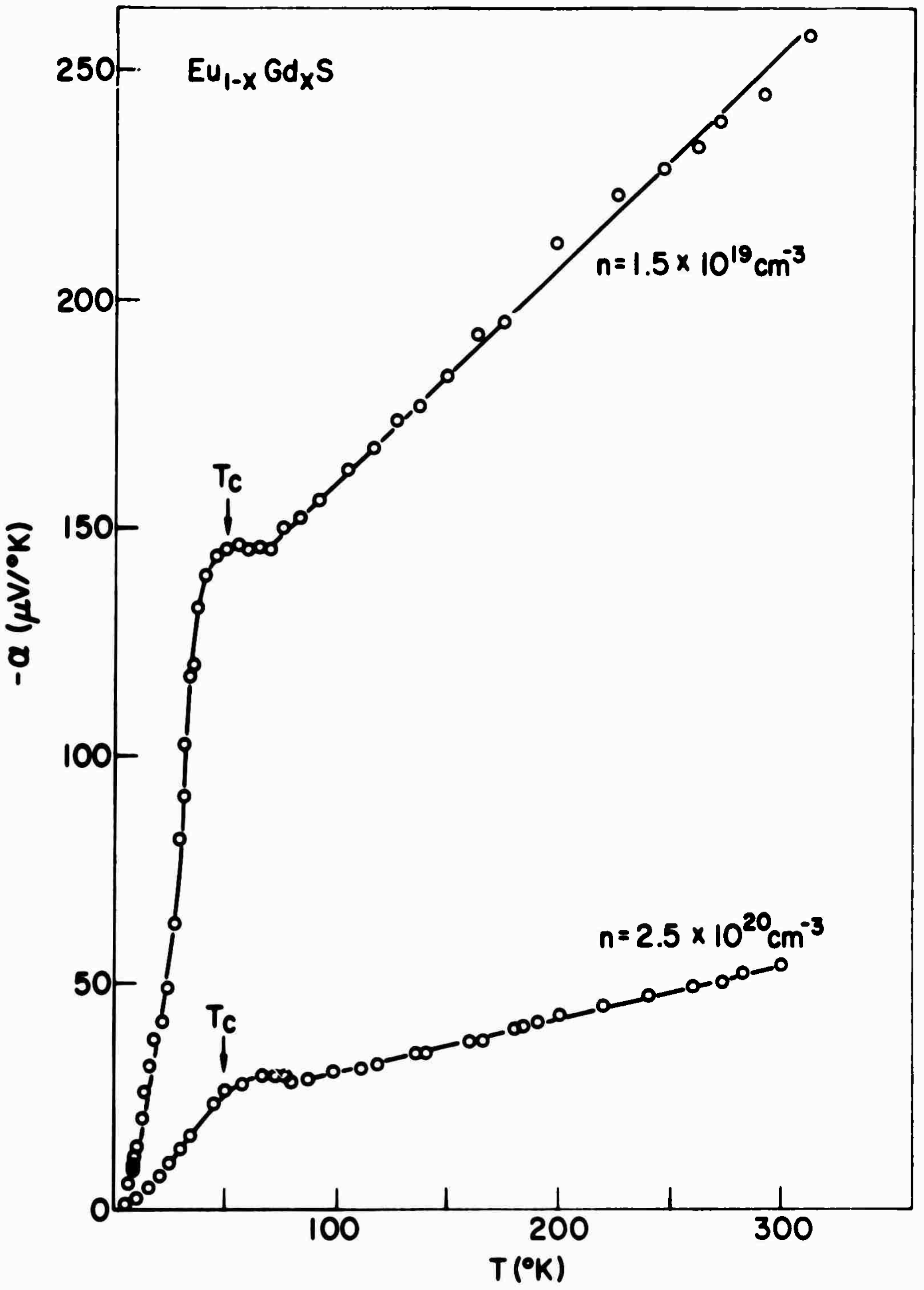

Figure 22: Seebeck coefficient α of $Eu_{1-x}Gd_xS$ with x = .03 (n = 2.5×10^{20} cm^{-3}) and x = .02 (n = $1.5 \times 10^{19} cm^{-3}$) as a function of temperature.

Observation ii) is not as yet explained. The critical scattering theory of De Gennes and Friedel[42] as well as refinements by Fisher and Langer[47] do not predict a resistivity peak near the Néel temperature for metals in which $k_F d \gg 1$, where k_F is the Fermi wave vector and d is the distance between spins. For the present sample of GdS this factor is $(3\pi^2 n)^{1/3}\, d = 3.8$ where n is the carrier concentration as measured by the Hall effect. The work of Maranzana,[48] which attempts to solve the Kondo problem in a concentrated spin lattice above the ordering temperature, predicts a peak in the resistivity near the Néel temperature, but the latter theory is at variance with the fact that a magnetic field (in this case the local exchange field) acting on the spins tends to quench the Kondo effect.[49] It should be pointed out, however, that experimental observations similar to ours have been made in other antiferromagnetic metals, notably, Dy and Er.[50] The Hall effect measured at 300°K in LaS and as a function of temperature in GdS is consistent with one electron per rare earth ion. From the Hall effect we derive carrier concentrations of $3.0 \times 10^{22}\,\mathrm{cm}^{-3}$ and $2.5 \times 10^{22}\,\mathrm{cm}^{-3}$ for GdS and LaS respectively, while the density of Gd and La ions is $2.0 \times 10^{22}\,\mathrm{cm}^{-3}$ and $2.3 \times 10^{22}\,\mathrm{cm}^{-3}$.

The analysis is similar for the degenerately doped $Eu_{1-x}Gd_xS$ samples but we were able to extract a value for u since, in addition to the other transport measurements, the temperature dependence of the Seebeck coefficient, α, was obtained. The results for two samples varying in carrier concentration by one order of magnitude are shown in Fig. 22. α varies approximately linearly with T from room temperature down to the transition temperature. There is an anomaly near T_c and a change in slope below T_c. Non-linearities at the lowest temperatures may be due to thermal emf's characteristic of the sample holder. We may, to first order in kT/E_F, use the expression for the Seebeck coefficient[51]

$$\alpha = \frac{-.0245\ T}{E_F(\mathrm{e.V.})}x \qquad (21)$$

where E_F is the Fermi energy and x is defined by $\sigma(E) = \text{constant}\ E^x$ where $\sigma = 1/\rho$ is the conductivity. For the special case that the electrons are described by a parabolic band $x = \frac{3+S}{2}$, where $\frac{S}{2}$ is the energy dependence of the relaxation time. If we, furthermore, neglect the variation with energy of all factors in $\sigma(E)$ other than $\tau_m(E)$ and $\tau_i(E)$ (the spin disorder and impurity scattering relaxation times respectively), both of which vary as $E^{-1/2}$ [42,52] then $x = 1$.[53] From this we obtain $E_F \approx .05$ eV for the Gd:EuS sample containing 1.5×10^{19} electrons/cc and $E_F \approx .2$ eV for the sample with 2.5×10^{20} carriers/cc. Since $kT \approx .025$, the analysis is not valid for the former (which accounts for the deviations of linearity near room temperature), but is a fair approximation for the more highly doped sample. If we set $k_F = (3\pi^2 n)^{1/3}$ and substitute $E_F = \frac{\hbar^2 k_F^2}{2um}$, the result is obtained that $u \approx .65$. This is a relatively small mass and suggests a broad band of electrons. The implications are far reaching. If the results of these admittedly crude approximations are valid, it is difficult to invoke a magnetic polaron model[54] to explain the giant magnetoresistance found in the low dopant concentration range for these materials.[22] The existence of magnetic polarons depends critically on the existence of a relatively narrow (<<1 eV) band of states.

In order to verify our value for u, we have analyzed infrared reflectivity data[55] taken on an EuS sample self-doped to 4.2×10^{19} electrons cm^{-3} and having a Hall mobility $\sim 17\ \mathrm{cm}^2\ \mathrm{volt}^{-1}\mathrm{sec}^{-1}$. A theoretical fit to the data was obtained with the use of classical free carrier dispersion expressions for the polarizability[56] and the results are shown in Fig. 23.

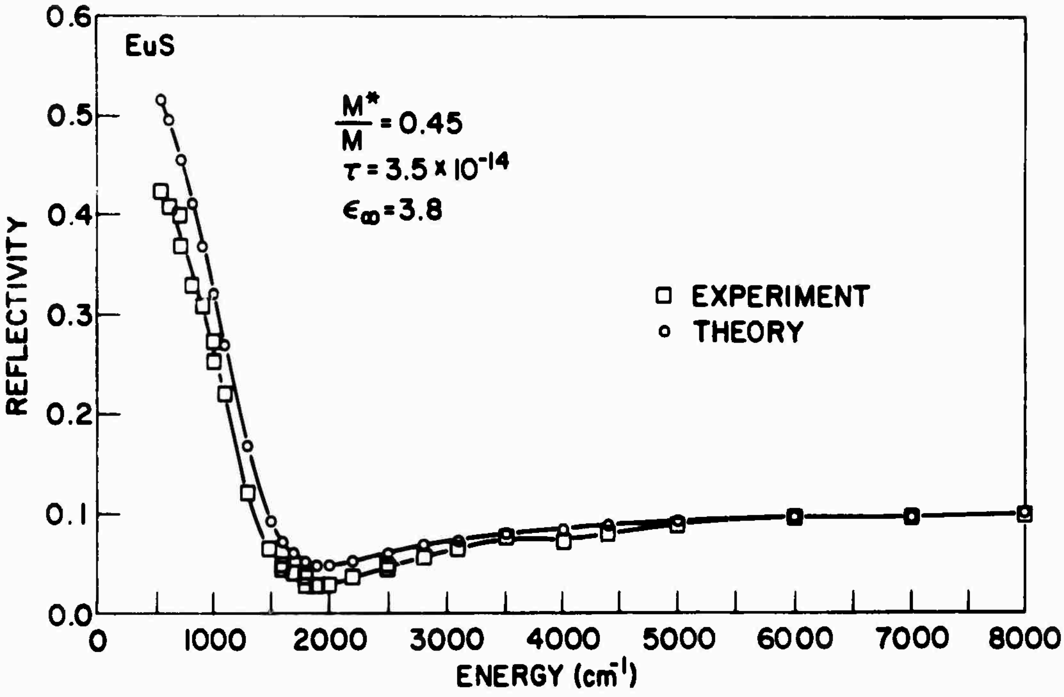

Figure 23: Observed and calculated reflectivity of EuS as a function of wave number.

The parameters giving the best fit were u = .45, $\tau = 3 \times 10^{-14}$ sec and the high frequency dielectric constant $\varepsilon_\infty = 3.8$. The values for u derived from the reflectivity and thermoelectric power data are in satisfactory agreement and indicate broad band behavior. $\varepsilon_\alpha = 3.8$ should be compared with the result of 5 ± .6 inferred from reflectivity data on the pure insulating material.[57]

The value obtained for τ requires further scrutiny. If we substitute the value for the room temperature resistivity of the Gd:EuS, as shown in Fig. 24, into the expression

$$\rho = \frac{1}{Ne\mu} = \frac{mu}{Ne^2\tau} \tag{22}$$

where e is the electronic charge and μ the mobility we obtain $\tau = 7.3 \times 10^{-15}$ sec. This value is smaller by a factor of ∿4 and not consistent with the reflectivity fit. Since we had assumed that the dominant energy dependence $\tau(E) \alpha E^{-1/2}$, the τ describing the infrared data might be expected to be smaller than the static one. Two explanations of the difference suggest themselves. First, the dispersion relation used in the fit did not include lattice dispersion whose contribution in the spectral region of interest may be considerable.[57] Second, a quantitative comparison of a self-doped EuS sample containing $\sim 4.2 \times 10^{19}$ carriers/cc with the Gd doped EuS sample containing 2.5×10^{20} carriers/cc may not be entirely justified.

The temperature dependence of ρ shown in Fig. 24 yields, with the use of Eq. 20, a magnetic contribution which is flat near room temperature ($\rho_\infty = 3.7 \times 10^{-4}\,\Omega$-cm) and rises to a value ∿3 times larger near the ferromagnetic ordering temperature, $T_c = 50$K. This behavior is well explained by the theories of spin disorder and critical scattering.[42] In fact, substi-

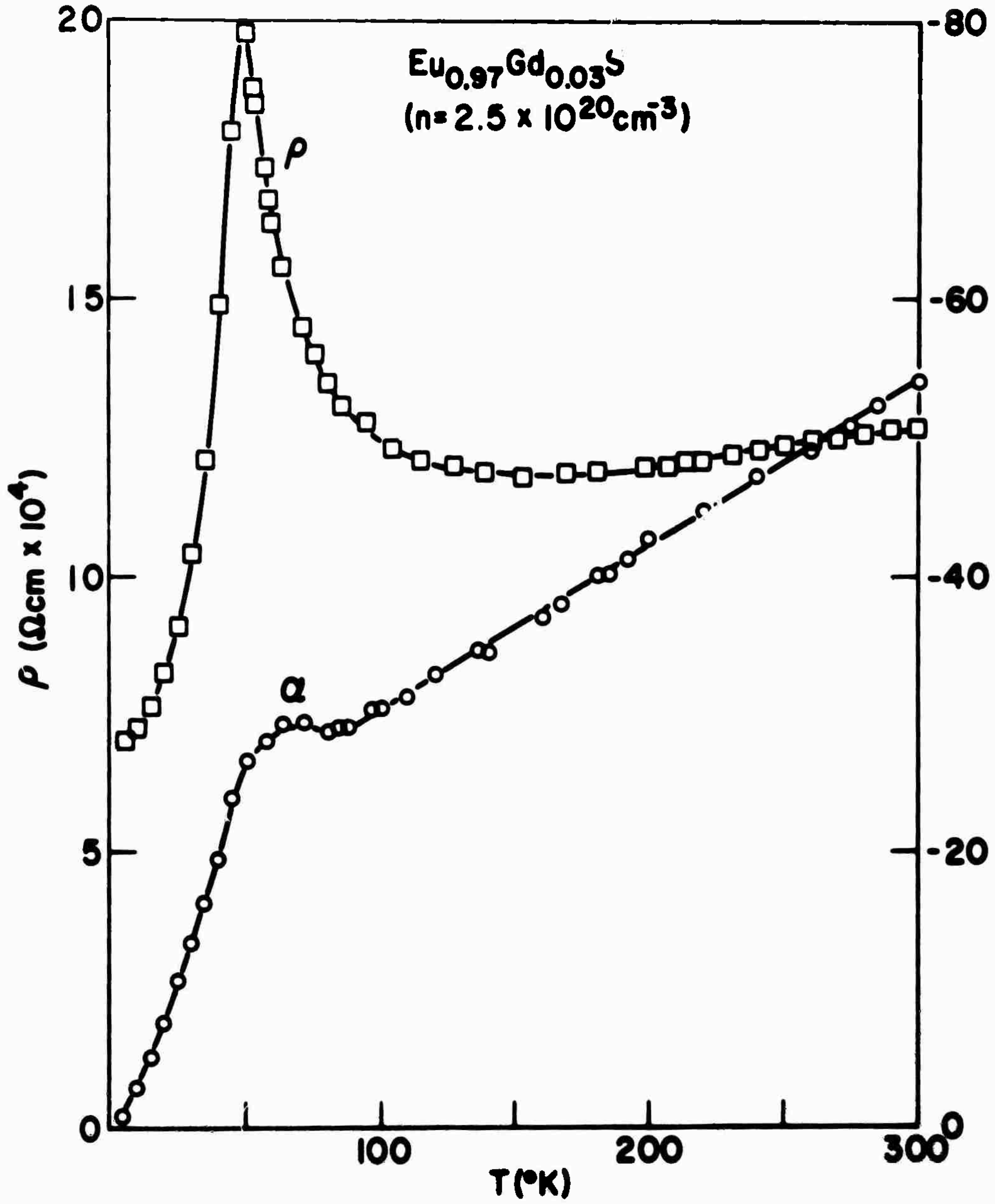

Figure 24: Resistivity ρ and Seebeck coefficient α of $Eu_{.97}Gd_{.03}S$ as a function of temperature.

tution into Eq. 19 yield $I_{c-f}(\mathrm{Eu}_{.97}\mathrm{Gd}_{.03}\mathrm{S}) \approx .07$ and $I_{c-f}(\mathrm{GdS})$ .03 eV, where $u = 1$ has been assumed for the latter calculation. These results are in order of magnitude agreement with independent measurements of J in connection with the metal insulator transition in EuO (See Sect. 3.3 of this report).

In conclusion we would like to stress that, according to the given experimental results and calculations based upon the assumption of a simple parabolic band, the exchange energy between conduction electrons and localized spins is of the same order of magnitude in GdS and EuS. This result is unexpected, since the atomic values for $I_{S-f} \approx .25\ I_{d-f}$ and, as mentioned earlier, the conduction band of GdS as seen with photoemission,[43] is d-like. Our results indicate the opposite trend, for example $I\ (\mathrm{Eu}_{.97}\mathrm{Gd}_{.03}\mathrm{S}) \approx 2\ I\ (\mathrm{GdS})$. A natural explanation may be found in the fact that observation, in general, is a function of the experiment. Thus, whereas photoemission is most sensitive to the highest density of states when electrons occupy overlapping bands, transport favours the most mobile carriers. It is, therefore, conceivable that in photoemission experiments in GdS[43] primarily d-like electrons are observed and in transport s-like electrons.

It is also clear from the results that the effective mass of the dominant carriers in Gd:EuS is smaller than the free electron mass. As we have stated earlier, this observation makes a magnetic polaron model an unlikely candidate to explain the very large resistivity peak near the magnetic ordering temperature in the doped rare earth sulfide and selenide systems.

REFERENCES

1. C. F. Guerci and M. W. Shafer, J. Appl. Phys., 37, 1406 (1966).
2. T. B. Reed and R. E. Fahey, 3rd Quarterly Report, Contract AF19(628)-5167, Lincoln Lab., Solid State Div., p. 15 (1969).
3. J. M. Haschke and H. A. Eick, J. Phys. Chem., 73, 374 (1969).
4. M. W. Shafer, J. Appl. Phys., 36, 1145 (1965).
5. L. Domage, J. Flahaut and M. Guittard, Compt. Rend., 246, 697 (1959).
6. M. W. Shafer and T. R. McGuire, J. Appl. Phys., 39, 588 (1968).
7. H. Preuner and W. Schupp, Z. Physik. Chem. 68, 157 (1949).
8. M. W. Shafer and C. F. Guerci, Abstract, 67th Annual Meeting, J. Am. Ceram. Soc., Philadelphia, 1965.
9. G. Petrich, private communication.
10. Mlle M. Guittard, Compt. Rend., 261, 2109 (1965).
11. R. Didchenko and F. P. Gortsema, J. Phys. Chem. Solids, 24, 863 (1963).
12. G. V. Samsonov, "High Temperature Compounds of Rare Earth Metals with Nonmetals " Consultants Bureau, New York, 1965.
13. A. Iandelli, Rare Earth Research, Ed. E. V. Kleeber, MacMillan, 1961, New York, Vol. 1, p. 135.
14. The data were collected by M. Frisch of the IBM Thomas J. Watson Research Center.
15. M. W. Shafer and J. C. Suits, J. Am. Ceram. Soc., 49, 261 (1966).
16. F. Holtzberg, T. R. McGuire, S. Methfessel and J. C. Suits, Phys. Rev. Letters, 13, 18 (1964).
17. F. Holtzberg, T. R. McGuire and S. Methfessel, J. Appl. Phys., 37, 976 (1966).

18. T. R. McGuire and M. W. Shafer, J. Appl. Phys., 35, 984 (1964).

19. T. R. McGuire, R. J. Gambino, S. J. Pickart and H. A. Alperin, J. Appl. Phys., 40, 1009 (1969).

20. T. R. McGuire and P. J. Flanders Chap. IV pages 128 and 132, "Magnetism and Metallurgy:" Editors A. Berkowitz and E. Kneller, Academic Press, New York and London, 1969.

21. T. A. Kaplan, Phys. Rev., 116, 888 (1959).

22. S. von Molnar and S. Methfessel, J. Appl. Phys., 38, 959 (1967).

23. T. Penney, Proc. Third Int. Conf. Photoconductivity, Stanford, August 1969, E. M. Pell ed., Pergamon, Oxford and New York, 1971, p. 133.

24. T. Kasuya and A. Yanase, Ref. Mod. Phys., 40, 1684 (1968).

25. A. Yanase and T. Kasuya, J. Phys. Soc. Japan, 25, 1025 (1968).

26. T. Kasuya, J. Appl. Phys., 41, 1090 (1970).

27. Section 3.3 is a summary of a more detailed publication: T. Penney and T. Kasuya, J. Appl. Phys., 42, 1403 (1971).

28. M. R. Oliver, J. A. Kafalas, J. O. Dimmock and T. B. Reed, Phys. Rev. Letters, 24, 1064 (1970).

29. M. R. Oliver, J. O. Dimmock and T. B. Reed, IBM J. Res. Develop., 14, 276 (1970).

30. M. R. Oliver, Thesis, Dept. of Electrical Eng., M.I.T., June 1970, unpublished.

31. G. Petrich, S. von Molnar and T. Penney, Phys. Rev. Letters, 26, 885 (1971).

32. L. J. van der Pauw, Philips Res. Repts., 13, 1 (1958).

33. M. J. Freiser, F. Holtzberg, S. Methfessel, G. D. Pettit, M. W. Shafer and J. C. Suits, Helv. Phys. Acta, 41, 832 (1968).

34. G. Busch, J. Appl. Phys., 38, 1386 (1967).
35. N. Menyuk, K. Dwight and T. B. Reed, Phys Rev. B, 3, 1689 (1971).
36. B. E. Argyle, N. Miyata and T. D. Schultz, Phys. Rev., 160, 413 (1967).
37. B. E. Argyle and N. Miyata, Phys. Rev., 171, 555 (1968).
38. S. von Molnar and T. Kasuya, Proc. Tenth Int. Conf. on Phys. Semiconductors, S. P. Keller, J. C. Hensel, F. Stern eds., Conf. 700 801, U.S. AEC Div. of Tech. Inf., Oak Ridge, Tenn., 1970, p. 233.
39. S. von Molnar and M. W. Shafer, J. Appl. Phys., 41, 1093 (1970).
40. M. Pollack and T. H. Geballe, Phys. Rev., 122, 1742 (1961).
41. See, e.g. S. von Molnar, IBM J. Res. Dev., 14, 269 (1970).
42. T. Kasuya, Prog. Theoret. Phys. (Kyoto), 16, 58 (1956); P. G. DeGennes and J. Friedel, J. Phys. Chem. Solids, 4, 71 (1958).
43. D. E. Eastman and Moshe Kuznietz, J. Appl. Phys., 42, 1396 (1971).
44. E. Gruneiseu, Ann. Physik, 16, 530 (1933).
45. V. L. Moruzzi and D. T. Teaney, Solid State Comm., 1, 127 (1963).
46. M. Blackman, Proc. Phys. Soc. (London), A64, 681 (1951).
47. M. Fisher and J. S. Langer, Phys. Rev., 20, 665 (1968).
48. F. E. Maranzana, J. Phys. Chem. Solids, 31, 2245 (1970).
49. We are grateful to Professor J. R. Schrieffer and Dr. T. D. Schultz for several valuable discussions on this point.
50. See, e.g. B. R. Coles, Adv. Phys., 25, 40 (1958).
51. N. F. Mott and H. Jones "The Theory of the Properties of Metals and Alloys," Dover Publications, Inc. (New York, 1958), p. 311.
52. C. Erginsoy, Phys. Rev., 79, 1013 (1950).

53. This is not a strong assumption, since lattice scattering (see Figure 4) which can have an energy dependence E^n with $-3/2 \le n \le 3/2$, represents only ~ 12% of the total at room temperature. This results in a maximum error of at most ± 15% in the effective mass.
54. T. Kasuya, A. Yanase and T. Takeda, Solid State Comm., 8, 1543 (1970).
55. We thank Dr. J. Torrance for making his data available to us before publication (this investigation is supported by ONR Contract N00014-70-C-0272).
56. See, e.g. J. R. Dixon, U. S. Naval Ordinance Laboratory Report No. NOLTR67-16 (1967).
57. J. D. Axe, J. Phys. Chem. Solids, 30, 1403 (1969).